



This is a repository copy of *A multiscale data reconciliation approach for sensor fault detection*.

White Rose Research Online URL for this paper:  
<https://eprints.whiterose.ac.uk/190548/>

Version: Accepted Version

---

**Article:**

Yellapu, V.S., Zhang, W., Vajpayee, V. [orcid.org/0000-0003-1179-7118](https://orcid.org/0000-0003-1179-7118) et al. (1 more author) (2021) A multiscale data reconciliation approach for sensor fault detection. *Progress in Nuclear Energy*, 135. 103707. ISSN 0149-1970

<https://doi.org/10.1016/j.pnucene.2021.103707>

---

© 2021 Elsevier Ltd. This is an author produced version of a paper subsequently published in *Progress in Nuclear Energy*. Uploaded in accordance with the publisher's self-archiving policy. Article available under the terms of the CC-BY-NC-ND licence (<https://creativecommons.org/licenses/by-nc-nd/4.0/>).

**Reuse**

This article is distributed under the terms of the Creative Commons Attribution-NonCommercial-NoDerivs (CC BY-NC-ND) licence. This licence only allows you to download this work and share it with others as long as you credit the authors, but you can't change the article in any way or use it commercially. More information and the full terms of the licence here: <https://creativecommons.org/licenses/>

**Takedown**

If you consider content in White Rose Research Online to be in breach of UK law, please notify us by emailing [eprints@whiterose.ac.uk](mailto:eprints@whiterose.ac.uk) including the URL of the record and the reason for the withdrawal request.



[eprints@whiterose.ac.uk](mailto:eprints@whiterose.ac.uk)  
<https://eprints.whiterose.ac.uk/>

# A Multiscale Data Reconciliation Approach for Sensor Fault Detection

Vidya Sagar Yellapu<sup>a,b</sup>, Weidong Zhang<sup>a,\*</sup>, Vineet Vajpayee<sup>c</sup>, Xinli Xu<sup>a</sup>

<sup>a</sup>Department of Automation, Shanghai Jiao Tong University, Shanghai 200240, China.

<sup>b</sup>Department of Electrical and Electronics Engineering, SRKR Engineering College, Bhimavaram 534204, India.

<sup>c</sup>School of Energy and Electronic Engineering, University of Portsmouth, Portsmouth, PO1 3DJ, UK.

---

## Abstract

When used separately on the sensor data of the processes like nuclear reactors, the data reconciliation with fault detection and isolation strategy gives noise-corrupted estimates, and the wavelet transformation gives erroneous inferences about the operating point of the process under sensor fault conditions. Aiming to solve these challenging problems, a hybrid multi-scale data reconciliation scheme that combines data reconciliation with the wavelet transform is proposed in this work. The proposed method uses the steady-state data reconciliation framework under the assumption of consistent algebraic relationships among the wavelet coefficient data. The role of multivariate techniques in obtaining the algebraic relationships, online detection and isolation of sensor faults, orthogonal decomposition, and reconciliation of the wavelet coefficients data is demonstrated. It is shown that the reconciled estimates obtained from this method very closely represent the true behavior of the process as problems with respect to random noise, high-frequency components due to process faults, sensor faults, and the influence of sensor faults on the signal estimates are alleviated. The effectiveness of this method is quantitatively established when applied to the ex-core neutron detector data of the advanced heavy water reactor in various simulations.

**Keywords:** Advanced heavy water reactor (AHWR), Data reconciliation, Ex-core neutron detectors, Fault detection and isolation (FDI), Ion chambers, Multiscale methods, Principal component analysis (PCA), Wavelets.

---

## 1. Introduction

In the operation of processes like nuclear reactors, safety, economy, reliability, and higher availability are the crucial requirements (Ma and Jiang, 2011). Control and protection systems deployed to meet these requirements act based on the measurement data of the key physical variables obtained from the sensors. For these systems to effectively perform their intended functionalities, the sensor data should be free from the errors, such as random errors or noise, and gross errors or faults (Li et al., 2020; Narasimhan and Jordache, 2000). Random errors contribute to the high-frequency components of the measured signal. They are usually small in magnitude and are unavoidable. On the other hand, sensor faults, which are generally large, bring in unwanted changes in the magnitude of signals. Both the random errors and faults lead to the erroneous representation of the operating state of the process being monitored. They can harm the functionalities of the control and protection systems. In the early stage of research, the random errors used to be smoothed with analog and digital filters, which introduce unwanted delay and spikes in the filtered response and require complicated tuning (Rhinehart, 1991; Weber, 1980; Oppenheim et al., 1997). Faults were dealt with by limit checking

and statistical quality control tests (Willsky, 1976; Maio et al., 2013) on the measured data and on their rate of change. These tests, however, give inaccurate outcomes when the steady-state of the process is disturbed. One more shortcoming with the early-stage methods is that they are applied separately on individual measurements, and thus, there is no scope for the utilization of interrelationships among the variables to improve the accuracy.

As a result of research in the past four to five decades, various data processing strategies and Fault Detection and Isolation (FDI) schemes of sensors are now available for reducing the effect of random errors and for the real-time monitoring of sensors so that the faulty readings can be discarded (Isermann, 2006; Venkatasubramanian et al., 2003c,a,b). Data Reconciliation (DR) is such a data processing strategy that achieves random error reduction by forcing the measurements to satisfy the interrelationships among the variables on which the measurements are made, called the process constraint model (Kuehn and Davidson, 1961; Narasimhan and Jordache, 2000). In this process, DR also gives scope for the estimation of the unmeasured and faulty variables as presented in Vaclavek (1969); Crowe et al. (1983) with the concept of projection matrix based on Q-R factorization (Noble and Daniel, 1977). In spite of the availability of the DR technique in linear, non-linear, steady-state, and dynamic versions (Narasimhan and Jordache, 2000), it can be stated from the results obtained in Yellapu et al. (2015b) and Yellapu et al. (2017) that a linear steady-state DR is sufficient for random error reduction for the cases in which

---

\*Corresponding author

Email addresses: vidyasagar.yellapu@gmail.com, yvsagar@sjtu.edu.cn (Vidya Sagar Yellapu), wdzhang@sjtu.edu.cn (Weidong Zhang), vineet.vajpayee@port.ac.uk (Vineet Vajpayee), xuxinli20061013@163.com (Xinli Xu)

the process is almost steady. This is due to the fact that the linear relationships among the variables are not much violated in nearly static processes. However, it should be noted that the use of DR is limited only to the case of sensor data corrupted with noise but not to the case of the data corrupted with sensor faults. For the DR to be effective in the latter case also, an FDI scheme should be used to know the source, time of occurrence, and magnitude of the fault(s) so that the effect of the fault(s) can be removed from the measurement data before feeding it to the DR scheme (Narasimhan and Jordache, 2000).

In the FDI methods now available, the major difference is the knowledge used for formulating the diagnostics. A model (either quantitative or qualitative) based FDI method uses the first principles for the generation of the residuals (Venkatasubramanian et al., 2003c,a); a data-based method (multivariate) relies on the process history (Venkatasubramanian et al., 2003b); and a signal-based one (univariate) employs time domain and frequency domain analysis on the signals (Venkatasubramanian et al., 2003b). All the FDI methods compare the actual measurements with the predicted measurements for the generation of features, which are subsequently used for the detection and diagnosis of faults. In general, the accuracy of FDI outcomes from the model-based methods is largely proportional to the complexity of the process knowledge, and sometimes it is not guaranteed even with very detailed knowledge. On the other hand, data-based and signal-based methods are easy to implement, less uncertain, and of no need for first principles' models. These methods yield very good outcomes when deployed in large processes such as large nuclear reactors, where a great many variables are measured using sensors (Hashemian, 2011; Uhrig and Tsoukalas, 1999; Upadhyaya et al., 2003; Yellapu et al., 2017; Mandal et al., 2017). Particularly, the data-based methods are quite suitable for sensor FDI as they can exploit the sensor data for further improving the accuracy and consistency through systematic data checking and treatment (Venkatasubramanian et al., 2003b).

The DR scheme is considered under either the model-based FDI or the data-based FDI based on the way the interrelationships among the variables (constraint model) to be embedded in the DR are obtained. For model-based FDI, the constraint model is obtained through the analysis of the process using first principles, while for data-based one, it is obtained with the empirical modeling using the process history. When there are a large number of variables to be interrelated, the multivariate statistical modeling technique named Principal Component Analysis (PCA) has been extensively used to cash on the benefits of the data-based methods (Kaistha and Upadhyaya, 2001; Upadhyaya et al., 2003; Lu and Upadhyaya, 2005; Zhao and Upadhyaya, 2006; Narasimhan and Shah, 2008; Razak et al., 2012; Yellapu et al., 2015b, 2017). PCA splits the multidimensional space spread by the process data into two subspaces that account for the major and minor variabilities. This splitting is helpful in knowing the onset of the faults through the use of  $T^2$  and Squared Prediction Error (SPE) or  $Q$  statistics (MacGregor et al., 1994; MacGregor and Kourti, 1995) as described in Kaistha and Upadhyaya (2001); Upadhyaya et al. (2003); Lu and Upadhyaya (2005); Zhao and Upadhyaya (2006). However,

a more detailed diagnosis like fault isolation and estimation of fault magnitude is possible based on the subspace representing the minor variability when a constraint model is developed from it and used in DR-based multivariate FDI framework (Yellapu et al., 2015b, 2017). The DR-based multivariate FDI supports the use of single fault identification strategies such as global (T, 1975), measurement (T, 1975), and nodal (Mah et al., 1976) tests, and multiple fault identification ones that use a variety of serial elimination and compensation strategies (Narasimhan and Jordache, 2000). Multiple fault identification strategies are more advantageous in terms of their ability to handle simultaneous faults in multiple locations. In this category, tests such as iterative measurement test, principal component test, and Generalized Likelihood Ratio Test (GLRT) (Narasimhan and Jordache, 2000; Yellapu et al., 2015c) are very popular. Of these, GLRT has an additional ability to estimate the fault magnitude, which can be further used for online fault correction. In spite of these advancements, the nature of the faults decides the accuracy of the outcomes from the FDI, and the treatment of slowly growing incipient faults is highly difficult as the faults in small magnitudes are masked by the random noise. One more drawback of the DR-based FDI of sensors is that the reconciled estimates are not completely free from the measurement noise. Making the situation in large processes like nuclear reactors more complex, vibrations induced by the process-faults also are superimposed on the measurement signals from the sensors (Hashemian, 2011). This complicates the sensor FDI and leads to erroneous outcomes from it. This necessitates the visualization of the sensor data at multiple scales so that sensor faults can be discriminated from the process faults.

There are various methods available in the literature for process-mode visualization in multiple scales like Multiscale PCA (MSPCA) (Bakshi, 1998), Multiscale Statistical Process Monitoring (Ganesan et al., 2004), Multiscale Latent Variable Regression (Nounou and Nounou, 2010), Multiscale Partial Least Squares (Madakyaru et al., 2017), Multiscale System Identification (Reis, 2009), and Multiscale Subspace Identification (Vajpayee et al., 2018). They are much suitable to aid in FDI in large systems with multiple simultaneously interacting modes and time-frequency localized phenomena. These techniques decompose the data into high-frequency and low-frequency components that respectively represent the periodical oscillations due to disturbances and process faults, and the true values of the variables being monitored. Generally, due to their very nature, signatures obtained from the high-frequency components facilitate in detecting the vibration-induced accidents, while those from the low-frequency components enable detection of the process changes and the sensor drifts (Dorr et al., 1997). An MSPCA based FDI scheme integrating wavelet transform with PCA (Jolliffe, 2002) for process and sensor-FDI as described in Yellapu et al. (2019) is found to be very effective in detecting the process-fault induced vibrations using the high-frequency detail coefficients and the sensor-faults using the low-frequency approximation coefficients with the help of the Generalized Likelihood Ratio Test (GLRT) (Narasimhan and Mah, 1987). The effectiveness of the scheme in Yellapu et al. (2019) is due to the contribution from the wavelets to re-

move the auto-correlation, and that from the PCA to remove the cross-correlation among the sensor signals. The novel approach of conducting sensor-FDI based on wavelet coefficients resulted in very good outcomes such as higher detection and identification rates even for very small sensor degradation and a very low Mean-Square Error (MSE) while estimating the fault magnitude quite accurately. This merit was due to the effect of random errors in the measurement data being very low in the approximation coefficients, which represent the low-frequency components of the measurement data averaged over a window whose length is specified by the wavelet decomposition level. This low-frequency phenomenon can be used to represent the true values of the variables on which measurements are made so that the control and protection of the process can be subsequently practiced. However, the accuracy of the sensor data corrupted by random errors and faults can be further enhanced by combining the multiscale framework with a DR-based approach for FDI.

Hence, in this work, a Multiscale DR (MSDR) approach, which is a hybrid scheme that combines the wavelet-based multiscale process mode visualization methodology with the steady-state DR plus the Q-R factorization is proposed. Similar to the MSPCA based sensor FDI scheme of Yellapu et al. (2019), the MSDR scheme of this work is also applied to the wavelet coefficients data obtained with the selection of a suitable decomposition depth for meeting the objectives such as differentiation of process faults from sensor faults and more quick yet accurate FDI compared to the regular FDI performed with single scale data. However, in contrast to the scheme of Yellapu et al. (2019), the proposed MSDR scheme has the additional ability to meet the objectives such as further reduction of the effect of random noise due to the DR, eliminating the effect of sensor-faults in the data, and the estimation of the faulty sensor signals. These features are unique to the proposed scheme with respect to the other works in the literature that are also based on the wavelet and GLRT-based FDI (Upadhyaya et al., 2014; Botre et al., 2017; Sheriff et al., 2017). In the proposed scheme, the FDI is done with GLRT due to its ace feature of estimation of the fault magnitude in addition to the fault isolation. The DR-based estimation of healthy and faulty sensor signals is done through Q-R factorization and the concept of the projection matrix. The constraint model, which acts as the backbone to the proposed method is obtained from PCA owing to its simplicity and its widespread use in the literature. With this framework, in a given sensor fault scenario, the MSDR approach can give higher detection and identification rates; and accurate estimates of the fault magnitudes, and those of the sensors even for smaller magnitudes of sensor faults. It is to be noted that though this approach can also handle the process-faults through variations in the frequency spectra noticed in the detail coefficients obtained with multiscale representation, the focus in this paper is laid only on the sensor faults.

The proposed MSDR scheme is applicable to systems in which there are multiple simultaneously interacting modes, time-frequency localized phenomena, and intermittent sensor faults. The Advanced Heavy Water Reactor (AHWR), a 920 MW (thermal), vertical, pressure tube type, heavy-water mod-

erated, boiling light-water cooled, natural circulation type reactor (Sinha and Kakodkar, 2006), represents such a system. The additional reasons for the suitability of the MSDR scheme to the AHWR are as follows: In a nuclear reactor, it is indeed the situation that all ex-core sensors will produce identical signals. One faulty ex-core sensor signal out of three sensor signals meant for one of the control and protection systems can be discarded by appropriate majority voting logic (Knoll, 2010). But faults masked by random errors, and simultaneous faults in multiple sensors, cannot be detected in this approach. The voting logic is helpful for reactive maintenance when the fault grows by a large value but not for the proactive one that can be done after the onset of the faults and before they develop as serious ones that can lead to a permanent outage of the sensors. In addition, the signal reconstruction for error reduction is not possible in the voting logic approach. On the other hand, the DR-based FDI is quite good at the detection and isolation of slowly developing faults with the help of the constraint model developed from the correlation among the sensor signals. Moreover, the accuracy of the reconciled estimates increases when more variables (sensor signals) are involved in the reconciliation process. The increased number of variables also allows handling multiple simultaneous faults in the sensors, which is not possible in the case of the voting logic-based approach for FDI. In this context, the role of the DR-based FDI system in monitoring the health of sensors while overcoming the issues with the voting logic is very much significant. Hence, the demonstration of the proposed MSDR approach for sensor fault detection is carried out on the simulated ex-core ion chamber (neutron sensor) signals of the AHWR. Different scenarios that combine events such as steady-state operation, abrupt and incipient faults in sensors, and a process change are considered, and the effectiveness of the proposed approach is numerically established.

The rest of the paper is organized as follows: Section 2 briefly discusses the key theoretical concepts such as the DR, PCA, GLRT, and the Q-R factorization. Section 3 gives the details of the MSDR and FDI based on the wavelet coefficients. Section 4 demonstrates the application of the proposed method to AHWR for the FDI of the ex-core ion chambers. Section 5 presents the results and discussion when the proposed method is applied to the ion chamber signals of the AHWR. Finally, conclusions are drawn in Section 6. Appendix Appendix A gives some mathematical insight regarding the reconciled estimates of the approximation coefficients.

## 2. Data Reconciliation, Principal Component Analysis, Generalized Likelihood Ratio Test, and Q-R Factorization

### 2.1. Data Reconciliation

When measurements are made on some physical variables  $\mathbf{x}_k$  belonging to a real-valued  $n$ -dimensional space  $\mathbb{R}^n$  at a time instant  $k$ , random natured measurement errors  $\boldsymbol{\varepsilon}_k \in \mathbb{R}^n$  are inevitable. The measurement vector can be written as  $\mathbf{y}_k = \mathbf{x}_k + \boldsymbol{\varepsilon}_k \in \mathbb{R}^n$ , when the measuring devices or sensors are assumed to be fault-free. DR technique reduces the effects

of random errors in the measurements  $\mathbf{y}_k$  by forcing them to be consistent with the known relationships about the process. In the case of the steady-state DR, the measurements are forced to obey the relationships among the variables  $\mathbf{x}_k$  embedded in a matrix  $\mathbf{A}$ , called the constraint model, as in

$$\mathbf{A}\mathbf{x}_k = \mathbf{0}, \quad (1)$$

and they are more accurate than the original measurements provided that the measurements are free from the sensor faults. The reconciled estimates are then given by

$$\hat{\mathbf{x}}_k = \mathbf{y}_k - \Sigma_{\varepsilon}\mathbf{A}^T(\mathbf{A}\Sigma_{\varepsilon}\mathbf{A}^T)^{-1}\mathbf{A}\mathbf{y}_k, \quad (2)$$

where  $\Sigma_{\varepsilon}$  is the covariance matrix of the random errors  $\varepsilon_k$ . However, when the DR is performed in the presence of sensor faults, estimates obtained from (2) will be erroneous being influenced by the fault magnitude. Hence, one of the statistical quality control tests or an FDI algorithm like GLRT (Narasimhan and Mah, 1987; Yellapu et al., 2019) must be used as a first step so that faulty measurements are eliminated from the DR problem and thus the effect of faults are reduced. It may also be noted that the model  $\mathbf{A}$  in (1) and (2) needs to be known beforehand either through the first-principles analysis of the process or through a data-based method like PCA (Yoon and MacGregor, 2004).

## 2.2. Principal Component Analysis

PCA identifies the model  $\mathbf{A}$  using the dependencies of a few variables in  $\mathbf{x}_k$  on the remaining variables. Generally, in any large process that involves many physical variables, it is common that some of the variables in  $\mathbf{y}_k$  made on physical variables of the process  $\mathbf{x}_k$  are redundant and are strongly correlated with the rest in  $\mathbf{y}_k$ . It is possible to estimate the values of the redundant variables from the measurements made on the other variables using the analytical redundancy (Narasimhan and Jordache, 2000). When the data collected on the variables in  $\mathbf{x}_k$  are placed as a cloud in  $\mathbb{R}^n$ , the major variability can be observed only in the  $(n - m)$  orthogonal directions, where  $m$  ( $m < n$ ) is the number of dependent variables in  $\mathbf{x}$ . DR-based FDI of sensors very much requires the  $m$  number of other orthogonal directions, the projection of the data onto which gives some negligible values, called the residuals, which are centered around the origin  $\mathbf{0} \in \mathbb{R}^n$ . With PCA, space  $\mathbb{R}^n$  can be decomposed into the  $(n - m)$  number of directions of major variability, called the principal component subspace, and  $m$  number of directions of insignificant variability that span the so-called residual subspace. This job is done by decomposing the data into eigenvalue and eigenvector pairs such that the magnitude of an eigenvalue shows the amount of variability along its corresponding eigenvector. When PCA is applied on the data collected on  $n \times N$  dimensional data matrix  $\mathbf{X} = [\mathbf{x}_1 \ \mathbf{x}_2 \ \dots \ \mathbf{x}_N]$ , where  $\mathbf{x}_k, \forall k = 1, 2, \dots, N$ , represents the true-data vector, the eigenvectors corresponding to zero-valued eigenvalues spread the residual subspace. The ordered set of such eigenvectors qualifies as the matrix  $\mathbf{A}$  in the relation (1).

However,  $\mathbf{X}$  is unknown but its approximately equivalent

matrix  $\mathbf{Y} = [\mathbf{y}_1 \ \mathbf{y}_2 \ \dots \ \mathbf{y}_N]$  is known, where  $\mathbf{y}_k \in \mathbb{R}^n, \forall k = 1, 2, \dots, N$ . The matrix  $\mathbf{Y}$  is decomposed in PCA as subspaces with major and minor variabilities based on the magnitude of the eigenvalues. In other words, the eigenvector matrix  $\mathbf{V}$  is partitioned as  $\mathbf{V} = [\mathbf{P} \ \mathbf{B}]$ , where  $\mathbf{P} = [\mathbf{v}_1 \ \mathbf{v}_2 \ \dots \ \mathbf{v}_{n-m}]$  represents the principal component subspace and  $\mathbf{B} = [\mathbf{v}_{n-m+1} \ \mathbf{v}_{n-m+2} \ \dots \ \mathbf{v}_n]$  represents the residual subspace. This can separate the deterministic variation (due to change in process) in  $\mathbf{Y}$  from the stochastic variation (due to noise). However, such projection requires the order of the residual subspace  $m$ , called the model order. Once it is known, the sample data vector at an instant  $k$  can be decomposed into the signal vector  $\hat{\mathbf{x}}_k$  and the noise vector  $\hat{\varepsilon}_k$  with the help of matrices  $\mathbf{P}$  and  $\mathbf{B}$  as follows:

$$\mathbf{y}_k = \mathbf{P}\mathbf{P}^T\mathbf{y}_k + \mathbf{B}\mathbf{B}^T\mathbf{y}_k = \hat{\mathbf{x}}_k + \hat{\varepsilon}_k. \quad (3)$$

The amount of disagreement of the data with the algebraic relationships among the sensors placed in the columns of  $\mathbf{B}$  are given by the constraint residuals vector  $\mathbf{r}_k \in \mathbb{R}^m$  as in

$$\mathbf{r}_k = \mathbf{B}^T\mathbf{y}_k = \mathbf{A}\mathbf{y}_k, \quad (4)$$

which has a mean value of  $\mathbf{0}$ , i.e.,  $E[\mathbf{r}_k] \simeq \mathbf{0}, \forall i = 1, 2, \dots, N$ . In (4), the matrix  $\mathbf{B}^T$  is taken equivalent to the constraint model  $\mathbf{A}$  that holds the relationships among the variables in the vector  $\mathbf{y}$ , since (4) resembles the relation (1) (Yellapu et al., 2015b).

## 2.3. FDI with the Generalized Likelihood Ratio Test

SPE or  $Q$  statistics (Lu and Upadhyaya, 2005; Misra et al., 2002) at any instant  $k$  can be computed based on the disagreement of the data  $\mathbf{y}_k$  with the relations in  $\mathbf{A}$  as given by

$$Q_k = \mathbf{y}_k^T(\mathbf{I} - \mathbf{P}\mathbf{P}^T)\mathbf{y}_k. \quad (5)$$

The SPE statistics in (5) can be used to take decisions about the sensor faults. For a false alarm probability  $\alpha$ , the threshold value to be set for the SPE statistic for declaring a sensor fault can be computed as (Botre et al., 2017)

$$Q_{\alpha} = g\chi_{\alpha,h}^2, \quad (6)$$

where  $g = \frac{\text{variance}(Q)}{2 \times \text{mean}(Q)}$  and  $\chi_{\alpha,h}^2$  is the value of chi-square distribution at a significance level of  $\alpha$  with degrees of freedom given by  $h = \frac{2 \times \text{mean}(Q)^2}{\text{variance}(Q)}$ . In online FDI of sensors, a fault is declared if  $Q_k$  computed from (5) exceeds the threshold  $Q_{\alpha}$ . However, the faulty sensor indices out of  $n$  variables in  $\mathbf{y}_k$  and the magnitude of faults can be investigated through the techniques such as GLRT that work based on the likelihood ratio of residuals and their probability distributions (Narasimhan and Jordache, 2000; Mandal et al., 2017; Yellapu et al., 2019; Botre et al., 2017).

In GLRT, the fault signature vectors  $\mathbf{f}_j = \mathbf{A}\mathbf{e}_j$  are formed for each sensor index  $j$ , where  $\mathbf{e}_j$  is the unit vector with 1 at position  $j$ . If  $g$  number of sensor faults are hypothesized, the fault signature matrix that holds the signature vectors as its columns

can be expressed as (Narasimhan and Jordache, 2000)

$$\mathbf{F}_i = \begin{cases} \mathbf{A}\mathbf{e}_{i_1}, & i_1 = 1, \dots, n; \\ \mathbf{A}(\mathbf{e}_{i_1}, \mathbf{e}_{i_2}), & \forall i_1, i_2 = 1, \dots, n, i_1 \neq i_2; \dots; \\ \mathbf{A}(\mathbf{e}_{i_1}, \mathbf{e}_{i_2}, \dots, \mathbf{e}_{i_g}), & \forall i_1, i_2, \dots, i_g = 1, \dots, n, \\ & i_1 \neq i_2 \neq \dots \neq i_g, \end{cases} \quad (7)$$

where the subscript  $i$  refers to the set of combinations in which  $i_1, i_2, \dots, i_g$  are chosen to exhaustively consider all possible combinations of number of simultaneous sensor-faults from  $1, 2, \dots, g$ . According to this, the residuals in (4) have a mean of  $\mathbf{0}$  and  $\mathbf{F}_i\mathbf{b}_k$  in the presence of no and  $g$  faults respectively, where  $\mathbf{b}_k$  is a column vector of unknown magnitudes of faults.

The Generalized Likelihood Ratio of the  $m$ -variate residuals given by (4) can be written as

$$\lambda(\mathbf{r}) = \sup \frac{p(\mathbf{r}|H_1)}{p(\mathbf{r}|H_0)}, \quad (8)$$

where  $p(\cdot)$  denotes the probability density function,  $H_0$  represents the null hypothesis stating that no fault is present, and  $H_1$  is the alternative hypothesis claiming that faults are present in one or more signals. When the residuals are assumed to follow a Gaussian probability density function, (8) can be written as

$$\lambda(\mathbf{r}) = \sup_{i, \mathbf{b}_k} \frac{\exp\left\{-\frac{1}{2}\mathbf{Q}_{i,k}^T \mathbf{\Sigma}_r^{-1} \mathbf{Q}_{i,k}\right\}}{\exp\left\{-\frac{1}{2}\mathbf{r}_k^T \mathbf{\Sigma}_r^{-1} \mathbf{r}_k\right\}}, \quad (9)$$

where  $\mathbf{Q}_{i,k} = \mathbf{r}_k - \mathbf{F}_i\mathbf{b}_k$ , and  $\mathbf{\Sigma}_r = \mathbf{A}\mathbf{\Sigma}_\varepsilon\mathbf{A}^T$  is the covariance matrix of the residuals. The maximum likelihood estimates of the fault magnitudes  $\hat{\mathbf{b}}_k$  are obtained by defining a variable  $L = 2 \ln \lambda(\mathbf{r}) = \sup_i L_{i,k}$ , where

$$L_{i,k} = \mathbf{r}_k^T \mathbf{\Sigma}_r^{-1} \mathbf{r}_k - \sup_{\mathbf{b}_k} \mathbf{Q}_{i,k}^T \mathbf{\Sigma}_r^{-1} \mathbf{Q}_{i,k}, \quad (10)$$

and by equating the first derivative of (10) with respect to  $\mathbf{b}_k$  to zero. The estimates of the fault magnitudes so obtained are

$$\hat{\mathbf{b}}_k = (\mathbf{F}_i^T \mathbf{\Sigma}_r^{-1} \mathbf{F}_i)^{-1} (\mathbf{F}_i^T \mathbf{\Sigma}_r^{-1} \mathbf{r}_k), \quad (11)$$

and the corresponding test statistics are

$$L_{i,k} = (\mathbf{F}_i^T \mathbf{\Sigma}_r^{-1} \mathbf{r}_k)^T (\mathbf{F}_i^T \mathbf{\Sigma}_r^{-1} \mathbf{F}_i)^{-1} (\mathbf{F}_i^T \mathbf{\Sigma}_r^{-1} \mathbf{r}_k). \quad (12)$$

The false alarm probabilities for each of the  $L_{i,k}$  are

$$\alpha_{i,k} = p(\chi_{g,\alpha}^2 \geq L_{i,k}), \quad (13)$$

where  $\chi_{g,\alpha}^2$  is a random variable following a chi-square distribution with  $g$  degrees of freedom. The combination  $i$  chosen out of  $\{i_1 = 1, \dots, n; i_1, i_2 = 1, \dots, n, i_1 \neq i_2; \dots; i_1, i_2, \dots, i_g = 1, \dots, n, i_1 \neq i_2 \neq \dots \neq i_g\}$  corresponding to the minimum false alarm probability gives the number and locations of faults and the fault magnitudes.

## 2.4. DR with Q-R factorization

For the reconciled estimates in (2) to accurately represent the true values  $\mathbf{x}_k$  of the same, the measurements from faulty sensors in  $\mathbf{y}_k$  are to be eliminated before DR is performed. The  $Q-R$  factorization (Noble and Daniel, 1977; Allaire and Kaber, 2008) with the help of a projection matrix constructed from the columns of  $\mathbf{A}$  corresponding to faulty sensors is useful in doing this (Narasimhan and Jordache, 2000). In this method, the overall estimation problem is divided into two sub-problems: one is the reconciliation of fault-free measurements and the other is the estimation of faulty signals, which are eliminated from the DR problem. The procedure is as follows:

If  $q$  out of  $n$  number of variables in  $\mathbf{x}_k$  are declared as faulty by an FDI method like GLRT, the vector  $\mathbf{x}_k$  can be decomposed into  $p = (n - q)$  number of healthy variables, denoted by  $\mathbf{x}_{h,k}$ , and  $q$  number of faulty variables, denoted by  $\mathbf{x}_{f,k}$ , and the constraint equation can be written as

$$\mathbf{A}_h \mathbf{x}_{h,k} + \mathbf{A}_f \mathbf{x}_{f,k} = \mathbf{0}, \quad \mathbf{x}_{h,k} \in \mathbb{R}^p, \quad \mathbf{x}_{f,k} \in \mathbb{R}^q, \quad (14)$$

where  $\mathbf{A}_h$  and  $\mathbf{A}_f$  are the columns of  $\mathbf{A}$  corresponding to  $\mathbf{x}_{h,k}$  and  $\mathbf{x}_{f,k}$ , respectively.  $Q-R$  decomposition is performed on the matrix  $\mathbf{A}_f$ , and matrices  $\mathbf{Q}_f$ ,  $\mathbf{R}_f$ , and  $\mathbf{\Pi}_f$  are obtained such that

$$\mathbf{A}_f \mathbf{\Pi}_f = \mathbf{Q}_f \mathbf{R}_f, \quad (15)$$

where  $\mathbf{\Pi}_f$  is the permutation matrix whose columns are permuted columns of a  $q$ -dimensional identity matrix such that

$$\mathbf{\Pi}_f^T \mathbf{x}_{f,k} = \begin{bmatrix} \mathbf{x}_{f_1,k} \in \mathbb{R}^{r_f} \\ \mathbf{x}_{f_2,k} \in \mathbb{R}^{(q-r_f)} \end{bmatrix}, \quad (16)$$

where  $r_f$  is the rank of matrix  $\mathbf{A}_f$ . Expressing

$$\mathbf{Q}_f = [\mathbf{Q}_{f_1} \quad \mathbf{Q}_{f_2}], \quad \mathbf{R}_f = \begin{bmatrix} \mathbf{R}_{f_1} & \mathbf{R}_{f_2} \\ \mathbf{0} & \mathbf{0} \end{bmatrix}, \quad (17)$$

where  $\mathbf{Q}_{f_1}$ ,  $\mathbf{Q}_{f_2}$ ,  $\mathbf{R}_{f_1}$  and  $\mathbf{R}_{f_2}$  are  $m \times r_f$ ,  $m \times (q - r_f)$ ,  $r_f \times r_f$  and  $r_f \times (q - r_f)$  matrices respectively, (14) can be written as

$$\mathbf{A}_h \mathbf{x}_{h,k} + [\mathbf{Q}_{f_1} \quad \mathbf{Q}_{f_2}] \begin{bmatrix} \mathbf{R}_{f_1} & \mathbf{R}_{f_2} \\ \mathbf{0} & \mathbf{0} \end{bmatrix} \begin{bmatrix} \mathbf{x}_{f_1,k} \\ \mathbf{x}_{f_2,k} \end{bmatrix} = \mathbf{0}. \quad (18)$$

By pre-multiplying the above equation by  $\mathbf{Q}_{f_2}^T$ , the following relations are obtained:

$$\mathbf{Q}_{f_1}^T \mathbf{A}_h \mathbf{x}_{h,k} + \mathbf{R}_{f_1} \mathbf{x}_{f_1,k} + \mathbf{R}_{f_2} \mathbf{x}_{f_2,k} = \mathbf{0}, \quad (19)$$

$$\mathbf{Q}_{f_2}^T \mathbf{A}_h \mathbf{x}_{h,k} = \mathbf{G}_h \mathbf{x}_{h,k} = \mathbf{0}, \quad (20)$$

where  $\mathbf{Q}_{f_2}^T$  is the projection matrix and  $\mathbf{G}_h = \mathbf{Q}_{f_2}^T \mathbf{A}_h$  is the reduced constraint model of the healthy measurements. From (20), the reconciled estimates of  $\mathbf{x}_{h,k}$  are obtained as

$$\hat{\mathbf{x}}_{h,k} = \mathbf{y}_{h,k} - \mathbf{\Sigma}_{\varepsilon_h} \mathbf{G}_h^T (\mathbf{G}_h \mathbf{\Sigma}_{\varepsilon_h} \mathbf{G}_h^T)^{-1} \mathbf{G}_h \mathbf{y}_{h,k}, \quad (21)$$

where  $\mathbf{y}_{h,k}$  is the measurement vector from the healthy sensors and  $\mathbf{\Sigma}_{\varepsilon_h}$  is the covariance matrix of  $\mathbf{y}_{h,k}$ . When  $\hat{\mathbf{x}}_{h,k}$  from (21) is substituted for  $\mathbf{x}_{h,k}$  in (19), the estimates of signals from the

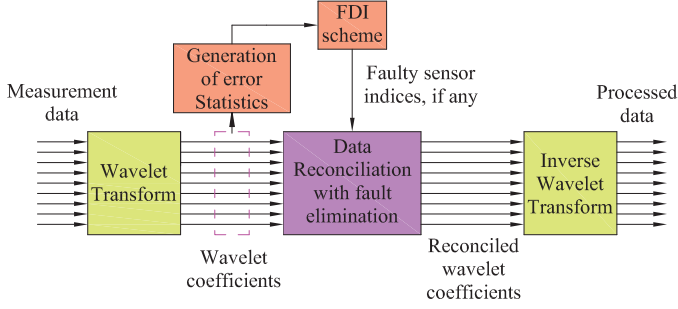


Figure 1: Online implementation of the proposed MSDR scheme

faulty sensors are obtained as

$$\hat{\mathbf{x}}_{f_1,k} = -\mathbf{R}_{f_1}^{-1} \mathbf{Q}_{f_1}^T \mathbf{A}_h \hat{\mathbf{x}}_{h,k} - \mathbf{R}_{f_1}^{-1} \mathbf{R}_{f_2} \hat{\mathbf{x}}_{f_2,k}. \quad (22)$$

The solution for  $\hat{\mathbf{x}}_{f_1,k}$  is based on two possible cases: If the rank of  $\mathbf{R}_{f_1} = r_f = q$ ,  $\mathbf{R}_{f_2}$  and  $\hat{\mathbf{x}}_{f_2,k}$  in (22) do not exist, all healthy and faulty variables are estimable, and a unique solution is possible. However, if  $r_f < q$ , a non-unique solution for  $\hat{\mathbf{x}}_{f_1,k}$  can be possible when the variables  $\hat{\mathbf{x}}_{f_2,k}$  are specified. In this work, estimates for  $\hat{\mathbf{x}}_{f_2,k}$  are taken as the corresponding reconciled values in (2). In either of these two cases, the vector of reconciled estimates  $\hat{\mathbf{x}}_k$  is obtained by suitably coupling the solutions for each variable from  $\hat{\mathbf{x}}_{h,k}$  and  $\hat{\mathbf{x}}_{f,k}$ .

### 3. Multiscale Data Reconciliation for On-line FDI

MSDR for on-line FDI involves different sequential operations on the multi-variate data: multiscale decomposition of measurement data using wavelets, the projection of the wavelet coefficients data onto the principal components for sensor FDI, DR and inverse wavelet transformation to get back the processed measurements (Bakshi, 1998; Yellapu et al., 2015b, 2017). These sequential operations are graphically illustrated in Fig. 1.

Since the wavelet function and the maximum depth of decomposition, denoted by  $J$ , play an important role in the effective implementation of wavelet-based techniques, they are selected as per the description given in Yellapu et al. (2019). That is, Haar wavelet is chosen, while  $J$  is selected using the concepts of Fourier transform and noise floor level (Reis, 2009; Vajpayee et al., 2018), as explained in Yellapu et al. (2019). After this, wavelet coefficients  $\mathbf{y}^w$  comprised of approximation (at scale  $J + 1$ ) and details (at scales  $j = 1, 2, \dots, J$ ) are computed from the time-series data  $\bar{\mathbf{y}} \in \mathbb{R}^{2^J \times 1}$ , as in

$$\mathbf{y}^w = \begin{bmatrix} \mathbf{y}_{J+1}^T & \mathbf{y}_J^T & \mathbf{y}_{J-1}^T & \cdots & \mathbf{y}_1^T \end{bmatrix}^T = \mathbf{W} \bar{\mathbf{y}}. \quad (23)$$

In (23),  $\mathbf{W}$  is the wavelet operator given by

$$\begin{aligned} \mathbf{W} &= \begin{bmatrix} \prod_{j=1}^J \mathbf{H}_j^T & \mathbf{G}_J^T \prod_{j=1}^{J-1} \mathbf{H}_j^T & \mathbf{G}_{J-1}^T \prod_{j=1}^{J-2} \mathbf{H}_j^T & \cdots & \mathbf{G}_1^T \end{bmatrix}^T, \\ &= \begin{bmatrix} \tilde{\mathbf{H}}_J^T & \tilde{\mathbf{G}}_J^T & \tilde{\mathbf{G}}_{J-1}^T & \cdots & \tilde{\mathbf{G}}_1^T \end{bmatrix}^T, \end{aligned} \quad (24)$$

where  $\tilde{\mathbf{H}}_J (1 \times 2^J)$  and  $\tilde{\mathbf{G}}_J (2^{J-j} \times 2^J)$  are matrices of wavelet

filter coefficients.

Based on these coefficients, the objectives of the MSDR-based FDI are met by a one-time executed off-line algorithm and a continuously running online one for every new observation (Yoon and MacGregor, 2004). The off-line algorithm is for obtaining the PCA-based constraint model, SPE thresholds ( $Q_\alpha$  computed from (6)), and the error covariance matrices. Once these are obtained, the online implementation is as follows (see Fig. 1): SPE statistics on the wavelet coefficients data are computed as in (5). When the SPE statistic on the approximation coefficients exceeds the threshold, a sensor fault is detected. For further diagnosis, the GLRT is executed whose outcomes are the faulty sensor index and the fault estimate. The GLRT outcomes are provided to the DR stage where the approximation coefficients are reconciled after the elimination of the faulty sensor from the estimation problem as explained in Section 2.4. It may be noted that a similar analysis on all the detail coefficients is prone to errors due to the fact that the detail coefficients carry noise dominated high-frequency information. Because of this, the constraint models developed on the noisy details can be misleading. Hence, the fault detection and isolation and the subsequent data reconciliation has been performed only on the approximation coefficients data. Nevertheless, the detail coefficients serve as indicators of process faults. Hence, significant detail coefficients (Vajpayee et al., 2018) i.e. detail coefficients that contain useful signal information are considered in the reconstruction of the signal to retain the useful high-frequency signal information.

For the evaluation of the proposed MSDR based scheme, the following indices are computed (Yellapu et al., 2015b):

1. *Overall Detection Rate (ODR)*: It is the percentage of detection of one or more faults or rejection of  $H_0$  out of the total number of trials. It involves detection, even during the cases where  $H_0$  is true. During the sensor faults, ODR is desirable to be close to 100% (Yellapu et al., 2015b).
2. *Overall Power (OP)*: It is the percentage of trials when one or more faults are correctly identified for a true  $H_1$ . OP should be close to 100% during the sensor faults (Yellapu et al., 2015b).
3. *Mean-Square Error (MSE)*: It is a measure of error in the estimate of fault magnitude  $\hat{\mathbf{b}}_k$  in a sensor, defined as

$$\sqrt{\frac{\sum_{k \in C} (\mathbf{b}_k - \hat{\mathbf{b}}_k)^T (\mathbf{b}_k - \hat{\mathbf{b}}_k)}{N_C}},$$

where  $C$  is the set of instants at which the faults are correctly identified,  $N_C$  is the cardinality of  $C$  and  $\mathbf{b}_k$  is the actual magnitude of the fault (Razak et al., 2012).

4. *Average Error Reduction (AER)*: Defining  $E_1 = \sum_{j=1}^{N_f} (\sum_{i=1}^n |y_{ij} - x_{ij}|)$  and  $E_2 = \sum_{j=1}^{N_f} (\sum_{i=1}^n |\hat{x}_{ij} - x_{ij}|)$ , the AER (Narasimhan and Mah, 1987) in percentage is given by

$$\text{AER} = \frac{(E_1 - E_2)}{E_1} \times 100, \quad (25)$$

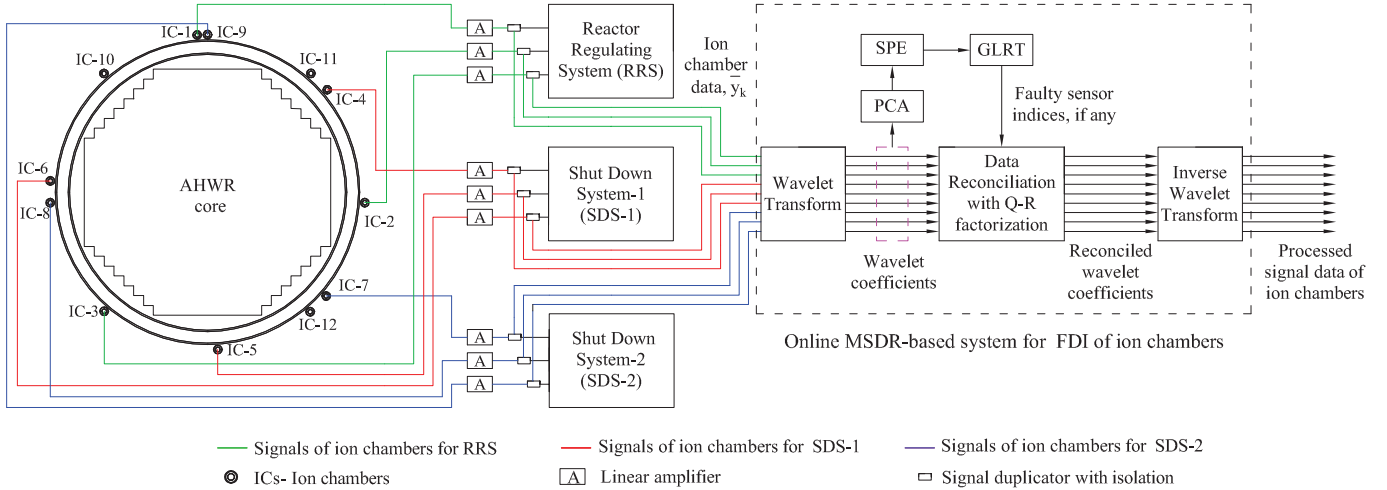


Figure 2: Implementation of the proposed MSDR-based method for sensor FDI in the AHWR.

where  $N_f$  is the number of observations in the data window with a sensor fault,  $y_{ij}$ ,  $x_{ij}$  and  $\hat{x}_{ij}$  are respectively the measurement, true and reconciled values of  $i^{\text{th}}$  sensor signal in the  $j^{\text{th}}$  observation.

#### 4. Application of MSDR-based FDI to Ion Chambers of AHWR

The application of MSDR-based FDI scheme to the AHWR (Sinha and Kakodkar, 2006; Yellapu et al., 2013) is discussed in this section. AHWR, being a large reactor, requires a large number of in-core and a good number of ex-core neutron detectors. Ion chambers are used as the ex-core neutron detectors, which are located in the vault water surrounding the reflector. There are nine ion chambers, out of which three ion chambers (namely, ion chambers-1, 2, and 3) are used for Reactor Regulating System (RRS) that controls and monitors the reactor, three ion chambers (namely, ion chambers-4, 5, and 6) are meant for Shut Down System-1 (SDS-1), and the remaining three (namely, ion chambers-7, 8 and 9) are for Shut Down System-2 (SDS-2). The linear amplifiers of the ion chambers produce a current signal, in the range of 4-20 mA, based on the magnitude of flux leaking into the vault water that is directly proportional to the core average flux. The online MSDR scheme is applied to the ion chamber signals obtained from their associated linear amplifiers.

The linear amplifier of an ion chamber  $-l$  produces a current signal given by (when the frequency components induced by the process faults are not present)

$$i_l = K\phi_l + \varepsilon_l + b_l + 4 \text{ mA}, \quad l = 1, 2, \dots, 9, \quad (26)$$

where  $K = 10.667$  is the product of detector sensitivity and the gain of the amplifier stages and  $\phi_l$  denotes the per-unit (p.u.) value of the local neutron flux at the  $l^{\text{th}}$  ion chamber location. In (26),  $\varepsilon_l$  is the random noise, and  $b_l$  is the sensor fault magnitude, if any, in the  $l^{\text{th}}$  ion chamber signal.

When  $i_l$  is arranged as the  $l^{\text{th}}$  element of the data vector  $y_k$ , as discussed in Section 2.1,  $\varepsilon_l$  becomes the  $l^{\text{th}}$  element of the random noise vector  $\varepsilon$ . The noise  $\varepsilon$  observed in ion chamber signals is generally independent being derived from a Gaussian distribution with the following properties (Yellapu et al., 2015a):

$$E[\varepsilon] = \mathbf{0}, \quad E[\varepsilon_k \varepsilon_l^T] = \mathbf{R} \delta_{k,l},$$

where  $\mathbf{R}$  is the covariance matrix of the measurement uncertainties, and  $\delta_{k,l}$  is the Kronecker delta.

As stated before, the aim of the proposed MSDR-based scheme is to reduce the ill effects of random errors and faults in an online fashion. Hence, its application to ion chambers of AHWR has to reduce or possibly eliminate the effects of  $\varepsilon_l$ , and  $b_l$  components from the ion chamber signal given by (26) so that it is possible to track the true value of the core-average flux closely. For this, the online MSDR-based scheme is implemented for FDI in AHWR as depicted in Fig. 2. The current signal data from the linear amplifiers of all the nine ion-chambers at an observation (before being fed to their respective control and protection systems) are supplied to the wavelet transformation and are decomposed into the approximation and detail coefficients. These coefficients are projected onto their respective PCA models so that SPE statistics are generated as in (5). The SPE statistics are tested against the threshold computed from (6). If the SPE doesn't exceed the threshold, the approximation coefficients are reconciled to smoothen the random errors. On the other hand, if SPE exceeds the threshold, GLRT is applied on the approximations to know the indices of the faulty ion chambers and the corresponding fault magnitudes. The reconciled estimates of the faulty and non-faulty ion chambers are obtained from the concepts of the Q-R factorization and the reduced DR. To obtain the MSDR-processed signals in the measurement space, the reconciled approximations and the significant details are subsequently inverse-wavelet transformed. The processed data closely represents the true data and it is then used for the control, protection, and monitoring purposes of the reactor.

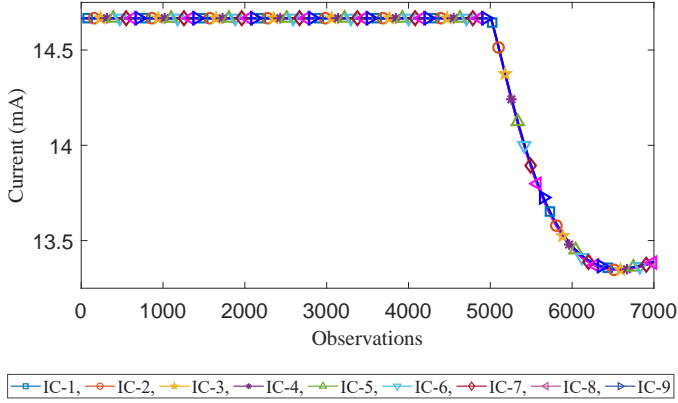


Figure 3: Ion chamber signals (true data without noise) during the transient corresponding to the demand power change.

## 5. Results and Discussion

The 17-node model developed for AHWR in Yellapu et al. (2013) is utilized in this work for the generation of the ion chamber signal data and thereby for the numerical illustration of the proposed MSDR approach for sensor FDI. The results obtained with the MSDR approach when applied to the ion chamber data during a demand power change transient are presented. It is assumed that the steady-state prevails in the reactor before the commencement of the demand power transient (Yellapu et al., 2013). The true values of the ion chamber signals are simulated for 140 s with a sampling time of 0.02 s, leading to the generation of 7000 observations on nine ion chambers. It is assumed that the demand power changes from 1.0 p.u. to 0.9 p.u. at the sampling instant  $k = 5000$  so that ion chamber signals vary to follow this change representing a process change of the reactor. The true values of all the nine ion chamber signals during this transient are as shown in Fig. 3. To make this data in Fig. 3 represent a realistic situation that prevails in an operating real-time reactor, a random noise derived from the Gaussian distribution with a standard deviation of 2% of the steady-state value of the ion-chamber signals (14.67 mA), *i.e.*  $0.02 \times 14.67 = 0.2933$  mA is considered (Yellapu et al., 2019; Yellapu et al., 2015b).

It may be noted that the decomposition depth,  $J$ , to be used for wavelet decomposition is computed as explained in Yellapu et al. (2019). Noisy signal data of ion chamber-1 available at the steady-state (the first 5000 samples) are chosen for this purpose. From the magnitude of the Fourier transform and the noise floor level, the maximum scale for decomposition is selected as  $J = 6$ . Accordingly, the wavelet transformation matrix  $\mathbf{W}$  for  $J = 6$  is built and the corresponding wavelet coefficients are used in the analysis.

It may also be noted that the first 1000 observations on all the nine ion chamber signals are used for off-line modeling. This is due to the process being at a fault-free steady-state, which is the required condition for error-free off-line modeling. As a part of off-line modeling, at all scales from  $J = 1, \dots, 6$ , wavelet coefficients are obtained from which the descriptive statistics, the PCA-based constraint model, and the SPE thresholds are

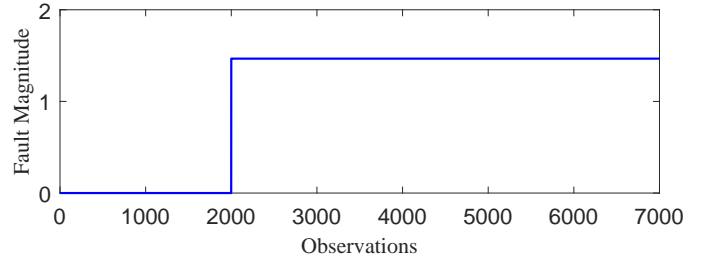


Figure 4: The magnitude of the sensor-fault magnitude (mA) in ion chamber-1.

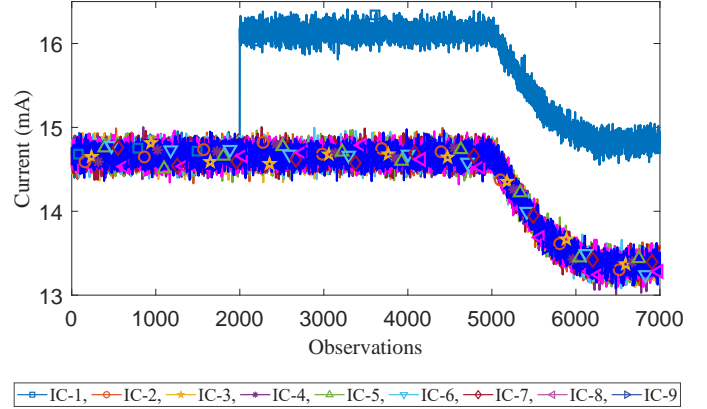


Figure 5: Ion chamber signals during the transient, when corrupted by the random noise and the sensor fault in ion chamber-1.

computed. These outcomes are subsequently used for online data processing and FDI.

In the demonstration of the working of the online MSDR scheme, sensor faults of abrupt and incipient nature are considered. The results obtained from the scheme in these two cases are presented of which the first case comprises a single-sensor fault (abrupt) case and the second one covers a double-sensor fault (one of abrupt and the other of incipient nature) case. These two cases also include scenarios of steady-state and the process change induced by the demand power change in common.

### 5.1. Single-sensor fault case

The ion chamber-1 is considered as the faulty sensor in this case. The fault is assumed to commence at observation index  $k = 2001$  with an abrupt nature. A bias of 10% of the nominal value of the signal at steady-state (14.67 mA) is considered as the fault magnitude as shown in Fig. 4. Due to the sensor fault, the ion chamber-1 signal abruptly deviates from the one that would have been obtained with no sensor fault. With this setup, the first 2000 samples are neither affected by any process change nor a sensor fault, samples from 2001 to 5000 are corrupted with the sensor fault of magnitude 1.46 mA and the remaining samples from 5001 to 7000 are under the influence of both the process change and the sensor fault. The simulated measurement data of ion chamber-1 corrupted by both the noise and the sensor fault is as shown in Fig. 5. This data is fed to the online MSDR-based system to obtain the wavelet coefficients

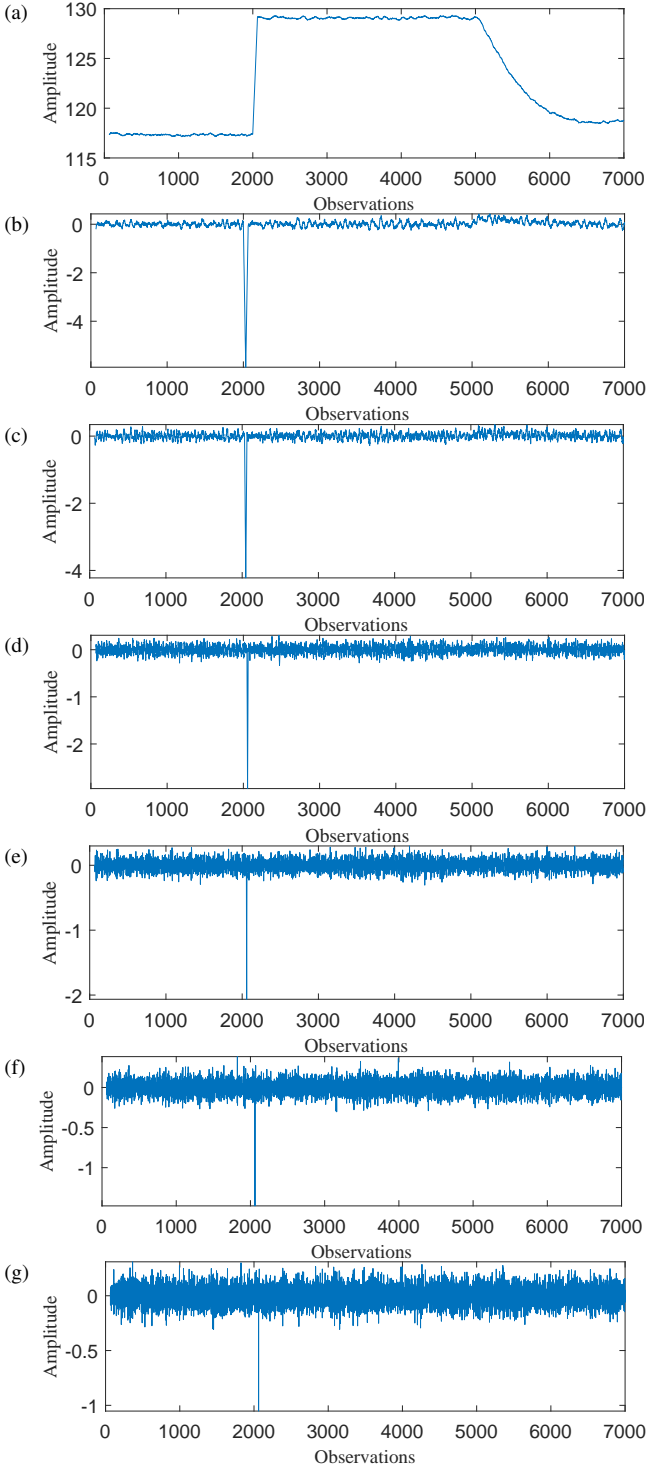


Figure 6: Unprocessed wavelet coefficients of ion chamber-1 in the single-sensor fault case: (a) approximation coefficients at level-6, (b) detail coefficients at level-6, (c) detail coefficients at level-5, (d) detail coefficients at level-4, (e) detail coefficients at level-3, (f) detail coefficients at level-2, and (g) detail coefficients at level-1.

at scales  $J = 1, 2, \dots, 6$ . The wavelet coefficients of the ion chamber-1 data are as shown in Fig. 6. A peak in the wavelet coefficients around sample number 2000 indicates the abrupt variation in the signal. The SPE statistics generated from the

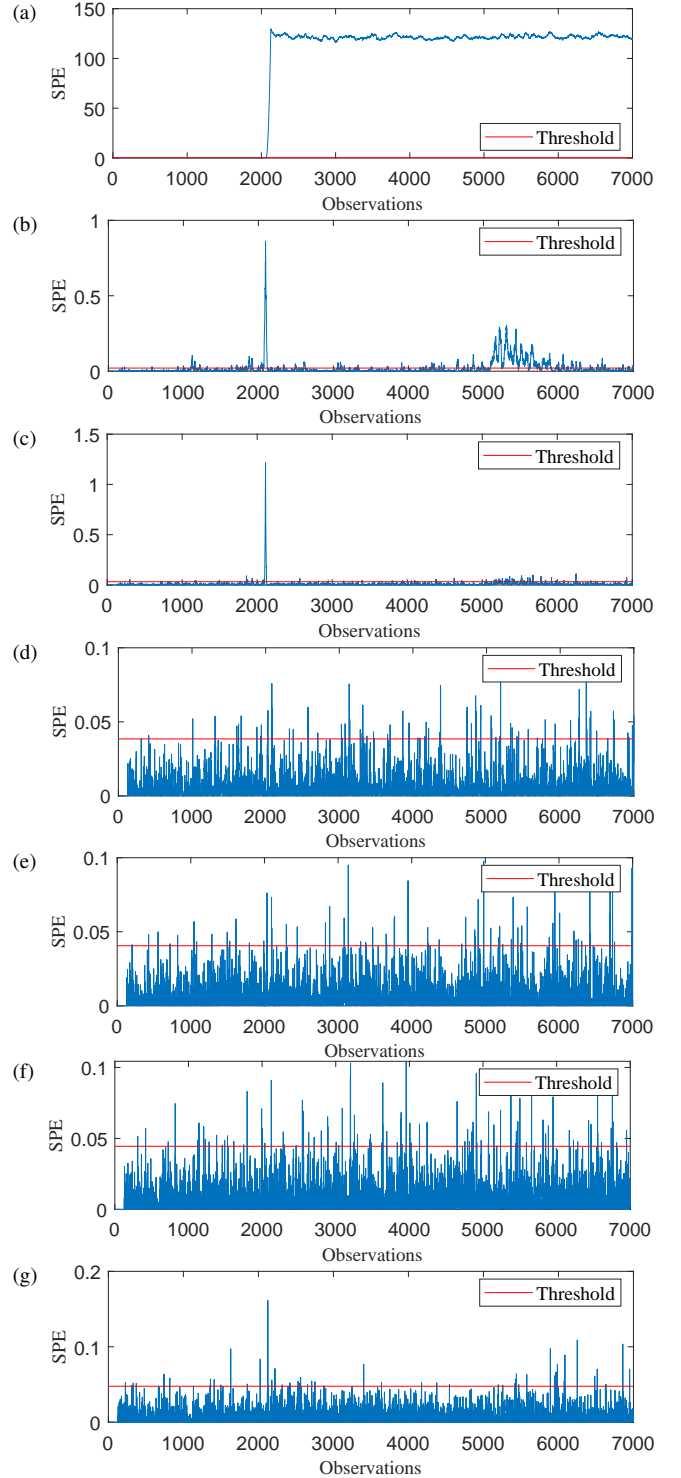


Figure 7: Single-sensor fault case: SPE computed from (a) approximation coefficients at level-6, (b) detail coefficients at level-6, (c) detail coefficients at level-5, (d) detail coefficients at level-4, (e) detail coefficients at level-3, (f) detail coefficients at level-2, and (g) detail coefficients at level-1.

projection of the wavelet coefficients on their respective PCA model are as shown in Fig. 7. From Figs. 6 and 7, it can be noted that the details at levels 5 and 6 contain significant signal information, and hence those levels are preserved for further processing in addition to the approximations. On the violation

of the SPE of wavelet coefficients near  $k = 2001$ , a fault is detected. Subsequently, fault isolation by GLRT is initiated to obtain the faulty sensor index and the fault magnitude. Based on the GLRT outcomes, the variable that is declared as faulty is eliminated from the DR problem with the help of Q-R factorization leading to a reduced DR problem. The reconciled approximation coefficients and the thresholded detail coefficients of ion chamber-1 data are as shown in Fig. 8. The reconciled estimates of the signals are shown in Fig. 9.

From Figs. 3 and 9, it is evident that the reconstructed data of the wavelet coefficients reconciled with FDI closely represent the true data of the ion chambers. The technical aspects that played a vital role in achieving this, *i.e.*, FDI outcomes namely index of the faulty sensor (ion chamber), and the estimate of the fault magnitude obtained with the approximation coefficients data, are as shown in Fig. 10. The SPE and the FDI outcomes obtained from the classical DR-based FDI on the other hand (performed on the original measurement data of Fig. 5) are as shown in Fig. 11. On comparing the Fig. 7(a) and Fig. 11(a), it becomes obvious that the abrupt nature of the sensor fault in ion chamber-1 is able to make the SPE exceed the threshold as soon as its commencement, in both the MSDR and the classical DR methods. This lead to the quick detection of the sensor fault and its eventual isolation with GLRT in both methods. But the accuracy in the fault estimate obtained with the MSDR approach outperformed that with the classical DR approach as evident from Fig. 10(b) and Fig. 11(c). It can also be noted that the accuracy in the fault estimate with the MSDR approach is persistent even when there is a process change from the 5001<sup>st</sup> observation. The indices for the evaluation of the proposed MSDR approach (refer to Sec. 3), namely ODR, OP, MSE, and AER, are also quantified and given for the cases of DR and MSDR methods in Table 1. These indices are computed for all the three sections of the data, *i.e.* steady-state (the first 2000 samples), steady-state with a sensor fault (samples from 2001 to 5000), and process change with a sensor fault (samples from 5001 to 7000). The superiority of the MSDR approach over the classical one for sensor FDI can be clearly observed from these indices as well. To describe, since no sensor fault is present in the steady-state, ODR, OP, and MSE are to be low, as is the case with the MSDR approach against the classical one. AER, which refers to the reduction of the effect of random errors in the reconciled data, is quite higher with the MSDR approach. In the data sections named as ‘steady-state with a sensor fault’ and ‘process change with a sensor fault’, since there is a sensor fault, the ODR and OP are required to be high, while the MSE in the fault estimate is to be low. AER is always required to be high in any case. All these requirements are met with the MSDR approach quite superiorly to the classical DR approach.

For the sake of comparison and for appreciating the role of the MSDR-based approach, various versions of ion chamber-1 data are plotted in Fig. 12. These versions are the noise-free true data, measurement data corrupted with noise and sensor fault, reconciled data obtained from the classical DR-based FDI, processed measurement data from the MSDR-based FDI based on the approximations coefficients only, and processed

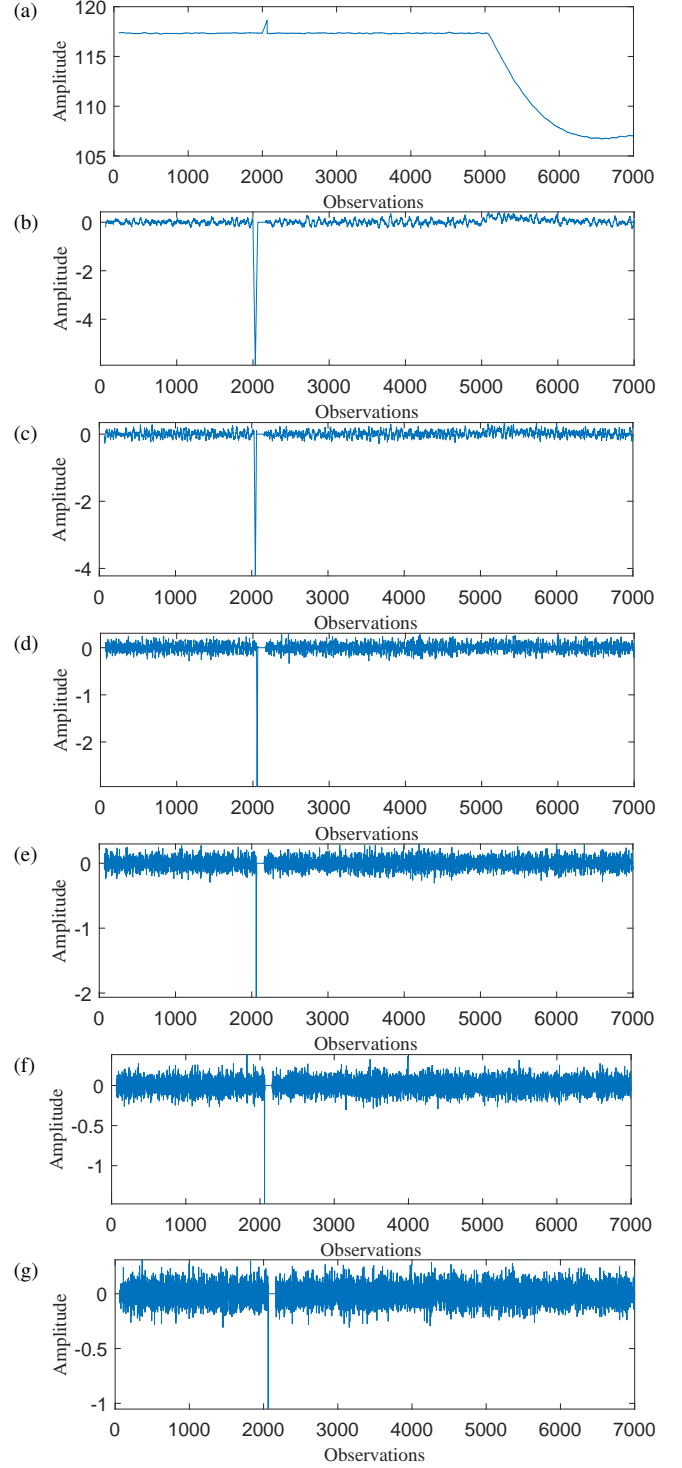


Figure 8: Processed wavelet coefficients of ion chamber-1 in the single-sensor fault case: (a) approximation coefficients at level-6, (b) detail coefficients at level-6, (c) detail coefficients at level-5, (d) detail coefficients at level-4, (e) detail coefficients at level-3, (f) detail coefficients at level-2, and (g) detail coefficients at level-1.

measurement data from the MSDR-based FDI based on the approximations and significant details coefficients. From Fig. 12, it can be said that the proposed MSDR approach could estimate the faulty signal very close to its true value even in the

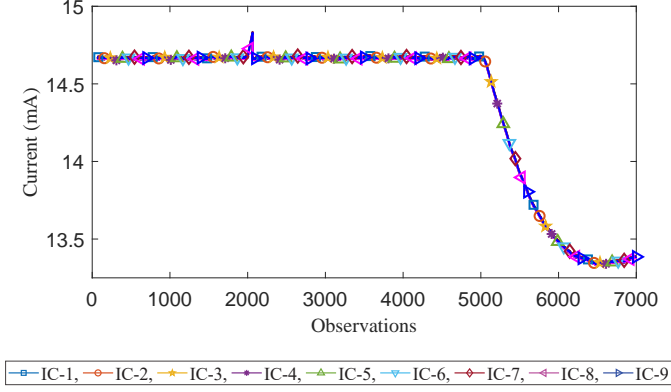


Figure 9: Single-sensor fault case: The processed data obtained with the retention of the significant scale details.

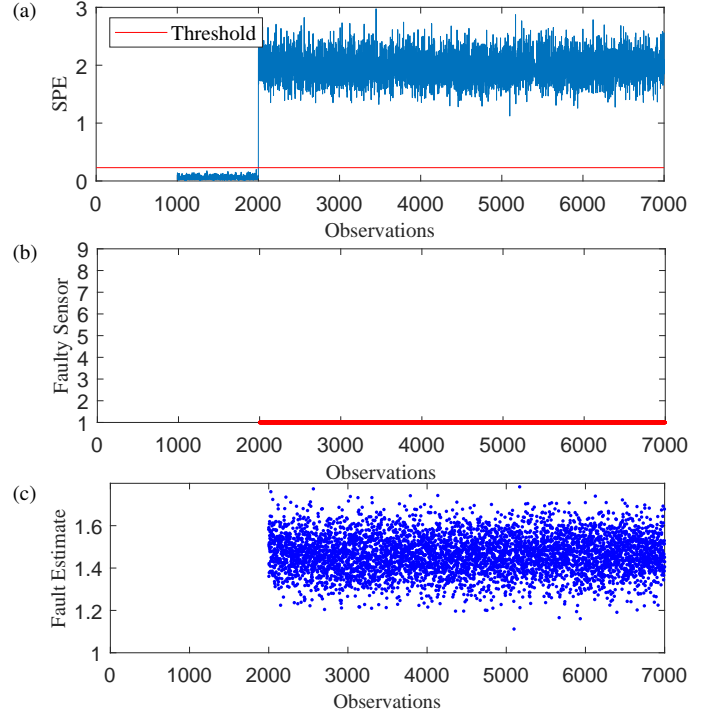


Figure 11: Classical DR-based FDI outcomes in single-sensor fault case: (a) SPE, (b) Faulty sensor index, and (c) Estimate of the fault magnitude (mA).

presence of random noise, sensor fault, and the process change. This means that the quality and accuracy of the measurement data has been very much enhanced with the proposed MSDR approach for sensor FDI.

## 5.2. Double-sensor fault case

The working of the MSDR scheme under more challenging conditions like sensor faults of both abrupt and incipient nature and a double-sensor fault scenario within and outside the steady-state process operation is demonstrated in this section. For this, while the rest of the conditions like an abrupt fault in ion chamber 1 and a process change are intact, an incipient sensor fault in ion chamber 5 is additionally considered whose time profile is as shown in Fig. 13. The ramp-natured incipient fault initiates at  $k = 3001$  or time  $t = 60$  s and sustains for the entire simulation. The fault magnitude changes with a monotonically increasing growth rate of 0.2% of the nominal value of the signal at steady-state (14.67 mA) per second. That is, the fault grows by a value of 2.934 A for every 100 s as shown in Fig. 13. With this, the first 2000 sample represent the steady-state, samples from 2001 to 3000 contain a sensor fault in ion chamber 1 data, those from 3001 to 5000 represent a double-sensor fault scenario (simultaneous faults in ion chambers 1 and 5), and those from 5001 to 7000 exhibit the double-sensor fault case along with a process change commencing at  $k = 5001$ . The ion chamber signals, in this case, are as shown in Fig. 14.

The processing of the signal shown in Fig. 14 is carried out in the same manner as explained in Section 5.1. The wavelet coefficients of the ion chamber-1 that would have been obtained if the MSDR-based FDI were not implemented are more or less

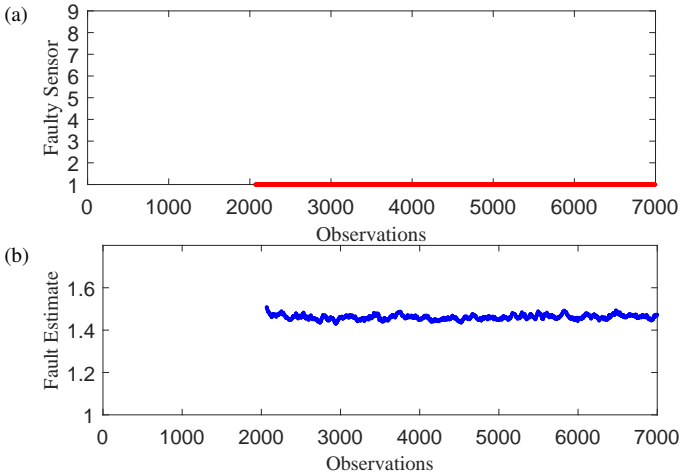


Figure 10: MSDR-based FDI scheme in single-sensor fault case: (a) Faulty sensor index, and (b) Estimate of the fault magnitude (mA).

Table 1: Single-sensor fault case: ODR (%), OP (%), MSE, and AER (%) in various data windows

Method	Index	Steady-state	Steady-state with a sensor fault	Process change with a sensor fault
Classical DR-based FDI	ODR	3.20	100	100
	OP	3.20	100	100
	MSE	0.08	0.09	0.09
	AER	66.67	88.98	88.71
MSDR-based FDI	ODR	0.05	100	100
	OP	0.05	100	100
	MSE	0.01	0.01	0.01
	AER	86.81	97.85	89.94

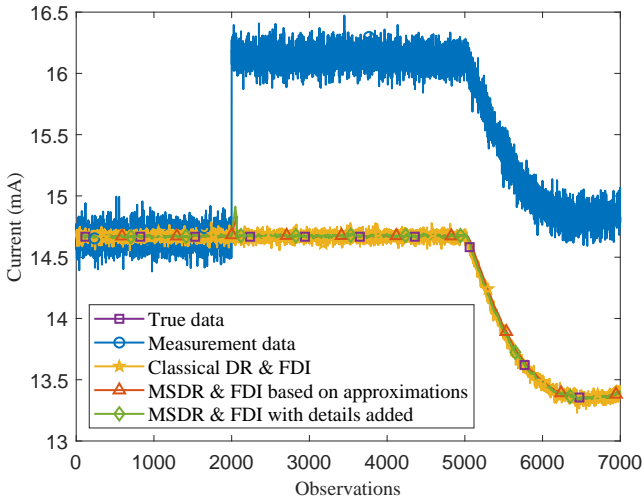


Figure 12: Single-sensor fault case: Various versions of ion chamber-1 data.

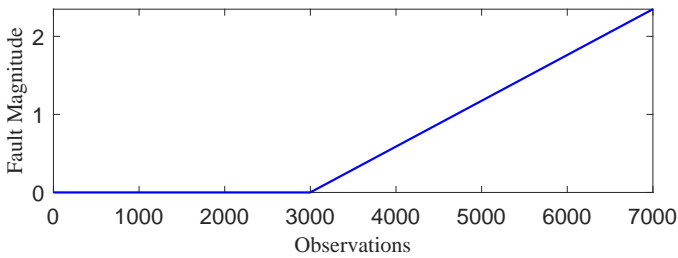


Figure 13: The growth of the sensor fault magnitude (mA) in ion chamber-5.

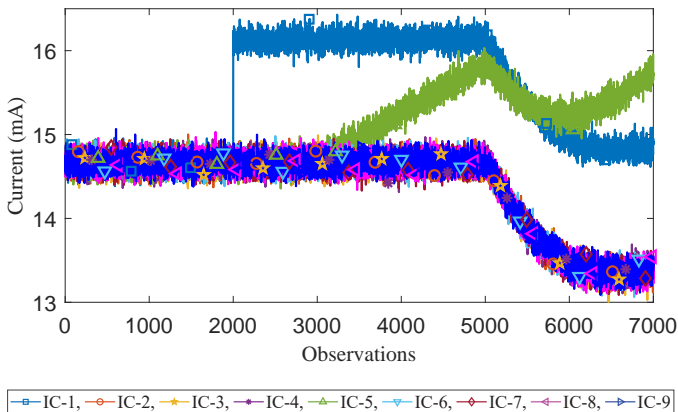


Figure 14: Ion chamber signals during the transient, when corrupted by the random noise and the sensor faults in ion chambers 1 and 5.

the same as those shown in Fig. 6. Those of ion chamber 5 are as shown in Fig. 15 in which the effect of the incipient fault in ion chamber 5 is seen in the high scale details 5 and 6. This result is not surprising as the fault in ion chamber 5 is slowly varying and thus it introduces only a lower frequency content in the details than the highest frequency contents added by the fast varying abrupt fault in ion chamber 1. The SPE profiles of the wavelet coefficients for this case are as shown in Fig. 16. The gradual departure of the SPE of the approximation coefficients from around  $k = 3001$  is due to the presence of the incipient fault in ion chamber 5. However, it is worth noting that the SPE of details at levels 5 and 6 are not responsive to the incipient fault, while they are to the abrupt one near  $k = 2001$ . The MSDR-based FDI processed wavelet coefficients of ion chamber 5 are shown in Fig. 17.

The SPE profile and the FDI outcomes obtained from the classical DR, in this case, are as shown in Fig. 18. The identification of the abrupt fault in ion chamber-1 is as prompt as its onset (at  $k = 2001$ ). But that of the incipient one in ion chamber-5 is delayed by around 500 samples from its onset (at  $k = 3001$ ) due to the overlapping effect of the random errors on the sensor fault. Contrastingly, the FDI outcomes from the MSDR scheme based on the SPE shown in Fig. 16(a) are as shown in Fig. 19 from which it can be said that the MSDR scheme has beaten the classical DR scheme in terms of speed of detection and the accuracy in the fault estimate. The superior performance of the proposed scheme can also be appreciated from the numerical values given in Table 2 as well. As before, various versions of ion chamber-1 and ion chamber-5 data in this case of double-fault scenario are plotted in Fig. 20 and Fig. 21 respectively. From Table 2, Fig. 20 and Fig. 21, it can be observed that the proposed MSDR approach could estimate the signals quite accurately despite the random noise, process change and sensor faults in two signals.

### 5.3. Discussion

The effectiveness of the proposed method is devoted to wavelets for removing the auto-correlation among the sensor signals, PCA for removing the cross-correlation, DR for further reduction of the effects of random errors in the wavelet coefficients, and FDI in eliminating the effects of faults. It should also be noted that the DR is based on the assumption that the measurement errors obey a known statistical distribution. In this work, a normal distribution is assumed for these errors basing on the central limit theorem, which states that the distribution of sample approximates a normal distribution as the sample

Table 2: Case of 2 sensor faults: ODR (%), OP (%), MSE, and AER (%) in various data windows

Method	Index	Steady-state	Steady-state with single sensor fault	Steady-state with two sensor faults	Process change with two sensor faults
Classical DR-based FDI	ODR	3.2	100	100	100
	OP	3.2	0	50.05	100
	MSE	0.09	0.08	0.09	0.09
	AER	66.28	89.32	72.72	46.66
MSDR-based FDI	ODR	0.05	99.80	100	100
	OP	0.05	0	97.20	100
	MSE	0.004	0.01	0.01	0.01
	AER	87.15	97.72	98.23	94.72

size becomes larger (Johnson and Wichern, 2002). The MSDR method can handle up to a maximum number of  $m$  (model order) sensor faults. This is due to the  $m$  being the degree of spatial redundancy, which acts as the backbone of the reconciliation (Romagnoli and Sanchez, 1999). Hence, the scheme can work successfully in all scenarios of multiple simultaneous faults whose number is less than  $m$ .

It is worth mentioning that the computation for a single observation on a computer with medium performance (1.6 GHz, Intel Core i5 quad-core CPU with 8 GB of RAM) took around 0.018 s, which is less than the considered sampling time of 0.02 s. Hence, the online implementation is ensured on certainly more performing dedicated machines mounted in the industrial control systems. In addition to this, since it is always possible to increase the sampling time in case of any online computational difficulty, it can be concluded that it is feasible to implement the proposed scheme online.

In ex-core sensor FDI applications of the proposed method, it should be noted that the ex-core sensors detect the core average flux, hence they produce identical signals with consistent correlation patterns among each other. The PCA-based constraint model is thus applicable to any other transient for which the same correlation pattern persists, as shown in Yellapu et al. (2015b). Hence, the superiority of the proposed MSDR scheme can be generalized for other transients like momentary perturbation of the control rods, refueling operation, and the like, though its working is illustrated under one transient involving demand power change. However, it should also be noted that it may not be possible to share the ion chamber signals from different systems meant for control and protection under the present operational and safety guidelines and practices followed by nuclear power plants. Hence, at the present juncture, the proposed scheme might be of use mainly at the supervisory level for operator decision support as well as for maintenance support.

## 6. Conclusion

An online MSDR scheme for reducing the effects of random errors and sensor faults from the measurement data of processes has been proposed. The scheme combines the multiscale features in the data with the constrained weighted-least-squares minimization problem for achieving this objective. The PCA is performed to identify the residual subspace and thus to arrive at the constraint model for the wavelet coefficients. Sensor faults are detected when the SPE statistics exceed the pre-defined threshold, followed by the GLRT for the sensor fault

isolation. DR with fault elimination is subsequently performed to obtain the reconciled estimates of the wavelet coefficients on which the inverse wavelet transformation is performed to get back the processed data. The MSDR scheme is numerically illustrated when applied to the ion chamber data of the AHWR. It has been revealed that the MSDR scheme is very effective in reducing the effects of random errors and sensor faults. FDI outcomes such as fault identification and fault estimate are also very good, even for very small fault magnitudes. The MSDR is also proved to be better in achieving its objectives than the classical DR scheme.

## Acknowledgements

This work was supported in part by the National Natural Science Foundation of China under Grant 61473183, Grant U1509211, and Grant 61627810, and in part by the National Key Research and Development Program of China under Grant 2017YFE0128500.

## Appendix A. The reconciled estimates of the approximation coefficients in fault-free case

The approximation coefficients obtained from the time series data of the measurements are given by the vector

$$\bar{\mathbf{a}}_k = \tilde{\mathbf{H}}_J \bar{\mathbf{y}}_k \in \mathbb{R}^n \quad (\text{A.1})$$

in which  $\tilde{\mathbf{H}}_J \in \mathbb{R}^{n \times 2^j n}$  is a matrix to obtain the approximation coefficients corresponding to each measured variable, and  $\bar{\mathbf{y}}_k \in \mathbb{R}^{2^j n \times 1}$  is a vector holding the data of all the  $n$  measured variables.  $\tilde{\mathbf{H}}_J$  can be mathematically represented as

$$\tilde{\mathbf{H}}_J = \begin{bmatrix} \tilde{\mathbf{H}}_J & \tilde{\mathbf{0}} & \dots & \tilde{\mathbf{0}} \\ \tilde{\mathbf{0}} & \tilde{\mathbf{H}}_J & \dots & \tilde{\mathbf{0}} \\ \vdots & \vdots & \ddots & \vdots \\ \tilde{\mathbf{0}} & \tilde{\mathbf{0}} & \dots & \tilde{\mathbf{H}}_J \end{bmatrix}, \quad (\text{A.2})$$

where  $\tilde{\mathbf{H}}_J$  is the vector corresponding to the approximation coefficients in the wavelet operator  $\mathbf{W}$ , and  $\tilde{\mathbf{0}}$  is a null vector  $\in \mathbb{R}^{1 \times 2^j}$ . The measurement vector  $\bar{\mathbf{y}}_k$  in (A.1) is given by

$$\bar{\mathbf{y}}_k^T = \left[ \bar{\mathbf{y}}_1^T \quad \bar{\mathbf{y}}_2^T \quad \dots \quad \bar{\mathbf{y}}_n^T \right], \quad (\text{A.3})$$

where  $\bar{\mathbf{y}}_i \in \mathbb{R}^{2^j \times 1}$ ,  $\forall i = 1, 2, \dots, n$ , is the time-series data of  $i^{\text{th}}$  measured variable.

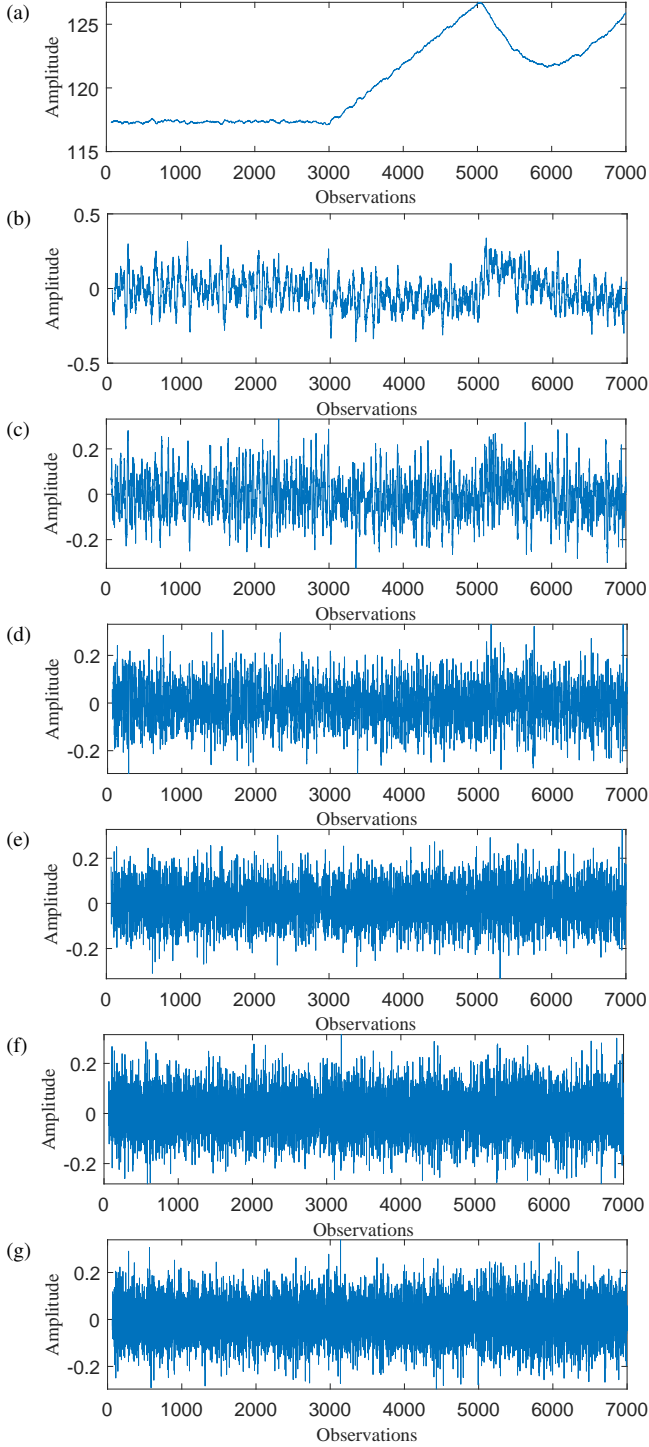


Figure 15: Unprocessed wavelet coefficients of ion chamber-5 in the double-sensor fault case: (a) approximation coefficients at level-6, (b) detail coefficients at level-6, (c) detail coefficients at level-5, (d) detail coefficients at level-4, (e) detail coefficients at level-3, (f) detail coefficients at level-2, and (g) detail coefficients at level-1.

If a Haar wavelet function is chosen, the vector  $\tilde{\mathbf{H}}_J$  for a chosen decomposition level  $J$  is

$$\tilde{\mathbf{H}}_J = \begin{bmatrix} \frac{1}{\sqrt{2^J}} & \frac{1}{\sqrt{2^J}} & \cdots & \frac{1}{\sqrt{2^J}} \end{bmatrix}. \quad (\text{A.4})$$

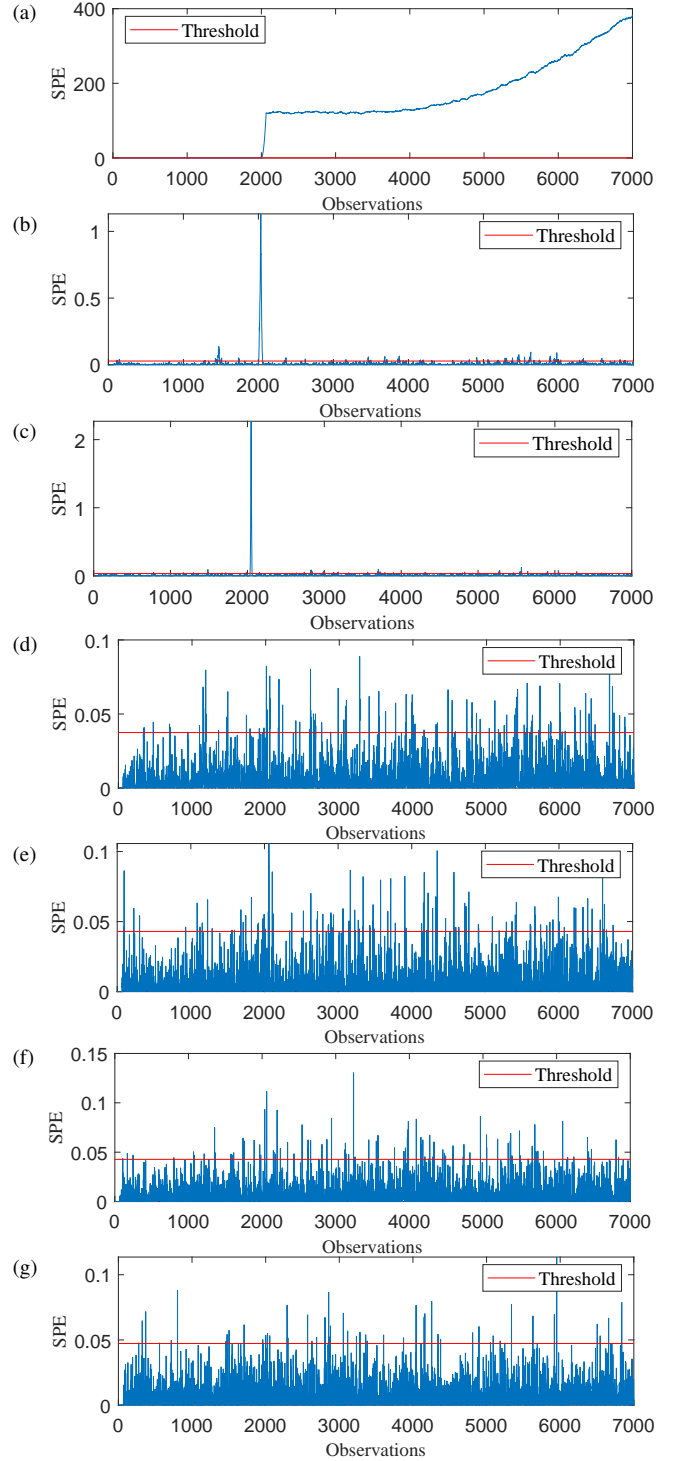


Figure 16: Double-sensor fault case: SPE computed from (a) approximation coefficients at level-6, (b) detail coefficients at level-6, (c) detail coefficients at level-5, (d) detail coefficients at level-4, (e) detail coefficients at level-3, (f) detail coefficients at level-2, and (g) detail coefficients at level-1.

Since the approximations are the weighted average of the time series data, their mean and variance get increased by  $\sqrt{2^J}$  times their respective values of the time-series data (Lemons et al., 2002). Hence, their probability distribution is  $N(\sqrt{2^J}\mu, \sqrt{2^J}\Sigma_\epsilon)$ . The reconciled estimates of the approxima-

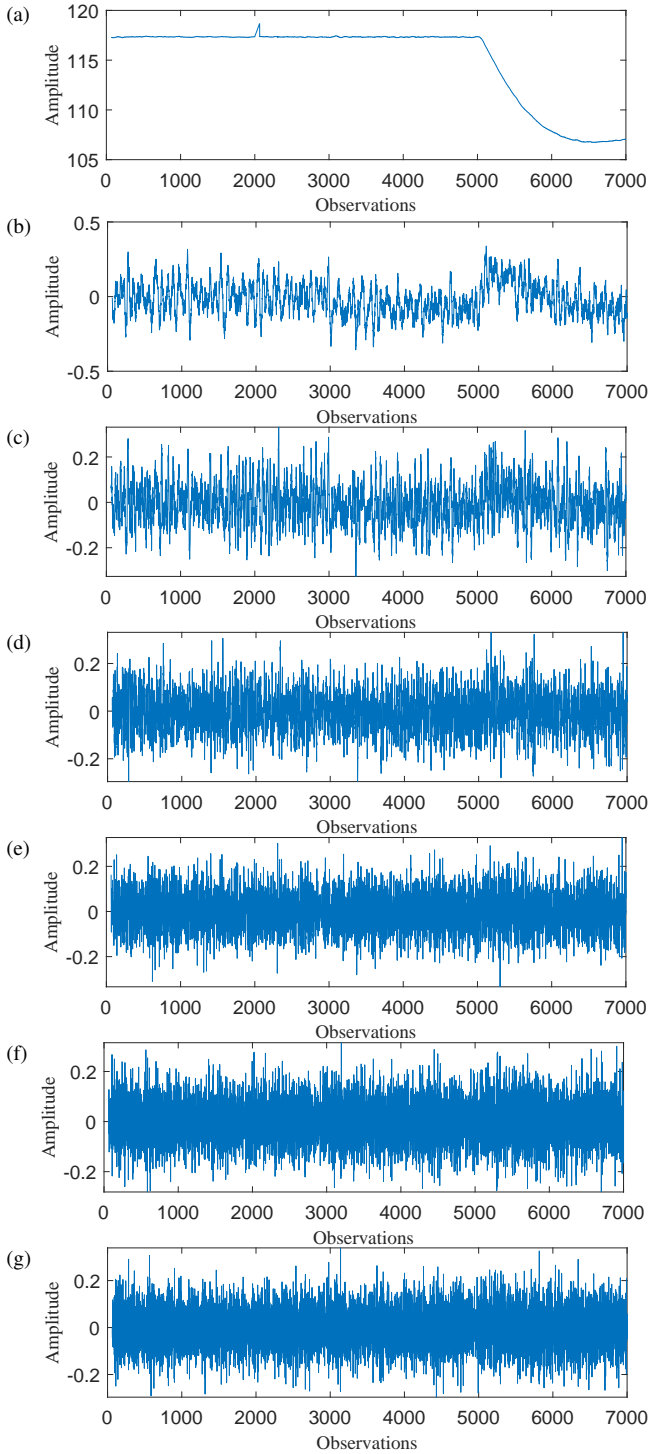


Figure 17: Processed wavelet coefficients of ion chamber-5 in the double-sensor fault case: (a) approximation coefficients at level-6, (b) detail coefficients at level-6, (c) detail coefficients at level-5, (d) detail coefficients at level-4, (e) detail coefficients at level-3, (f) detail coefficients at level-2, and (g) detail coefficients at level-1.

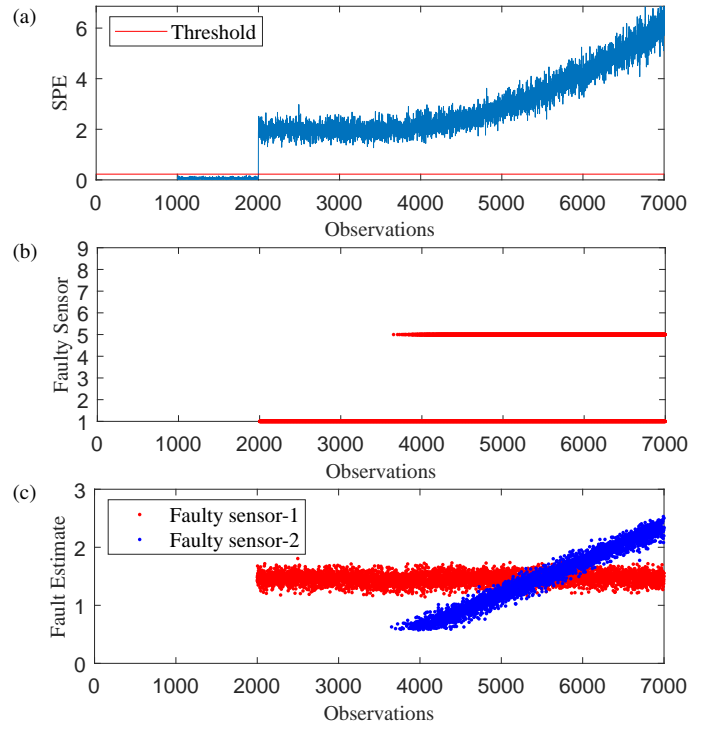


Figure 18: Case of 2 sensor faults: Sensor-FDI outcomes with the classical DR: (a) SPE, (b) Faulty sensor indices, and (c) Estimate of the fault magnitude (mA).

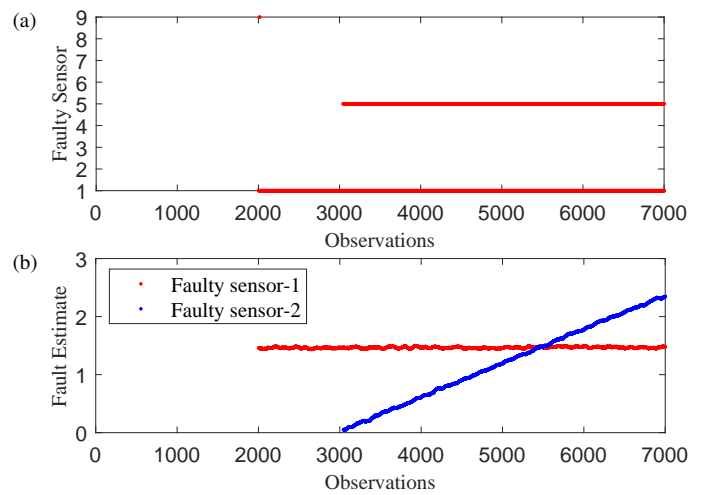


Figure 19: Case of 2 sensor faults: Sensor-FDI outcomes with MSDR: (a) SPE, (b) Faulty sensor index, and (c) Estimate of the fault magnitude (mA).

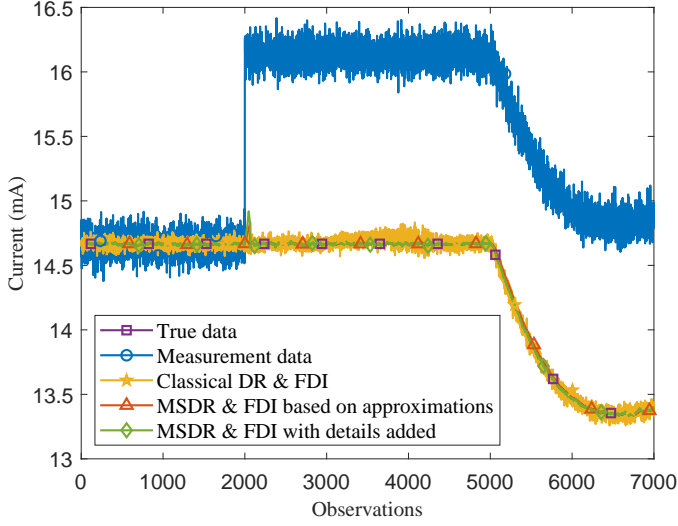


Figure 20: Case of 2 sensor faults: Various versions of ion chamber-1 data.

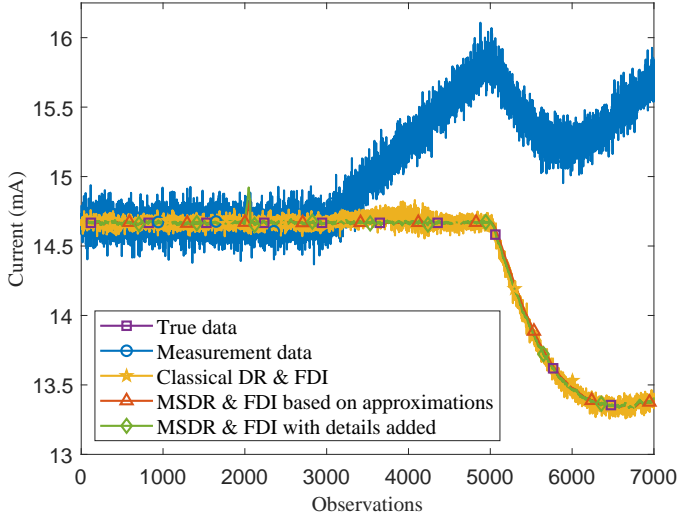


Figure 21: Case of 2 sensor faults: Various versions of ion chamber-5 data.

tions are thus given by (Narasimhan and Jordache, 2000; Kuehn and Davidson, 1961)

$$\hat{\mathbf{a}}_k = \bar{\mathbf{H}}_J \bar{\mathbf{y}}_k - \Sigma_\varepsilon \mathbf{A}_A^T (\mathbf{A}_A \Sigma_\varepsilon \mathbf{A}_A^T)^{-1} \mathbf{A}_A \bar{\mathbf{H}}_J \bar{\mathbf{y}}_k, \quad (\text{A.5})$$

where  $\mathbf{A}_A$  is the PCA-based constraint model obtained from approximation coefficients in the off-line modeling process. Ex-

panding the terms,

$$\hat{\mathbf{a}}_k = \frac{1}{\sqrt{2^J}} \begin{pmatrix} \sum_{\theta=k-2^J+1}^k \bar{y}_{\theta,1} \\ \sum_{\theta=k-2^J+1}^k \bar{y}_{\theta,2} \\ \vdots \\ \sum_{\theta=k-2^J+1}^k \bar{y}_{\theta,n} \end{pmatrix} - \Sigma_\varepsilon \mathbf{A}_A^T (\mathbf{A}_A \Sigma_\varepsilon \mathbf{A}_A^T)^{-1} \mathbf{A}_A \begin{pmatrix} \sum_{\theta=k-2^J+1}^k \bar{y}_{\theta,1} \\ \sum_{\theta=k-2^J+1}^k \bar{y}_{\theta,2} \\ \vdots \\ \sum_{\theta=k-2^J+1}^k \bar{y}_{\theta,n} \end{pmatrix}. \quad (\text{A.6})$$

## References

- Allaire, G., Kaber, S. M., 2008. Numerical Linear Algebra. Springer.
- Bakshi, B. R., 1998. Multiscale PCA with application to multivariate statistical process monitoring. *AIChE J.* 44 (7), 1596–1610.
- Botre, C., Mansouri, M., Karim, M. N., Nounou, H., Nounou, M., 2017. Multiscale pls-based glrt for fault detection of chemical processes. *Journal of Loss Prevention in the Process Industries* 46, 143 – 153.
- Crowe, C. M., Campos, Y. A. G., Hrymak, A., 1983. Reconciliation of process flow rates by matrix projection. part I: Linear case. *AIChE J.* 29 (6), 881–888.
- Dorr, R., Kratz, F., Ragot, J., Loisy, F., Germain, J. ., Jan 1997. Detection, isolation, and identification of sensor faults in nuclear power plants. *IEEE Transactions on Control Systems Technology* 5 (1), 42–60.
- Ganesan, R., Das, T. K., Venkataraman, V., 2004. Wavelet-based multiscale statistical process monitoring: A literature review. *IIE Transactions* 36 (9), 787–806.
- Hashemian, H. M., 2011. On-line monitoring applications in nuclear power plants. *Progress in Nuclear Energy* 53 (2), 167 – 181.
- Isermann, R., 2006. Fault-Diagnosis Systems: An Introduction from Fault Detection to Fault Tolerance. Springer, Darmstadt.
- Johnson, R. A., Wichern, D. W., 2002. Applied multivariate statistical analysis. Prentice Hall, USA.
- Jolliffe, I. T., 2002. Principal Component Analysis. Springer Series in Statistics. Springer.
- Kaitha, N., Upadhyaya, B. R., 2001. Incipient fault detection and isolation of field devices in nuclear power systems using principal component analysis. *Nuclear Technology* 136 (2), 221–230.
- Knoll, G. F., 2010. Radiation Detection and Measurement. John Wiley & Sons.
- Kuehn, D. R., Davidson, H., 1961. Computer control II. mathematics of control. *Chem. Eng. Progress* 57, 44–47.
- Lemons, D., Langevin, P., Gythiel, A., 2002. An Introduction to Stochastic Processes in Physics. Johns Hopkins Paperback. Johns Hopkins University Press.
- Li, D., Wang, Y., Wang, J., Wang, C., Duan, Y., 2020. Recent advances in sensor fault diagnosis: A review. *Sensors and Actuators A: Physical* 309, 111990.
- Lu, B., Upadhyaya, B. R., 2005. Monitoring and fault diagnosis of the steam generator system of a nuclear power plant using data-driven modeling and residual space analysis. *Ann. Nucl. Energy* 32, 897–912.
- Ma, J., Jiang, J., 2011. Applications of fault detection and diagnosis methods in nuclear power plants: A review. *Prog. Nucl. Energy* 53 (3), 255 – 266.

- MacGregor, J. F., Jaeckle, C., Kiparissides, C., Koutoudi, M., 1994. Process monitoring and diagnosis by multiblock PLS methods. *AIChE J.* 40 (5), 826–838.
- MacGregor, J. F., Kourti, T., 1995. Statistical process control of multivariate processes. *Control Eng. Practice* 3 (3), 403–414.
- Madakyaru, M., Harrou, F., Sun, Y., 2017. Improved data-based fault detection strategy and application to distillation columns. *Process Safety and Environmental Protection* 107, 22 – 34.
- Mah, R. S. H., Stanley, G. M., Downing, D. M., 1976. Reconciliation and rectification of process flow and inventory data. *Ind. Eng. Chem. Proc. Des. Dev.* 15 (1), 175–183.
- Maio, F. D., Baraldi, P., Zio, E., Seraoui, R., Dec 2013. Fault detection in nuclear power plants components by a combination of statistical methods. *IEEE Trans. Reliability* 62 (4), 833–845.
- Mandal, S., Santhi, B., Sridhar, S., Vinolia, K., Swaminathan, P., 2017. Sensor fault detection in nuclear power plant using statistical methods. *Nucl. Eng. and Design* 324, 103 – 110.
- Misra, M., Yue, H., Qin, S., Ling, C., 2002. Multivariate process monitoring and fault diagnosis by multi-scale pca. *Comp. & Chem. Eng.* 26 (9), 1281 – 1293.
- Narasimhan, S., Jordache, C., 2000. *Data Reconciliation & Gross Error Detection: An Intelligent Use of Process Data.* Gulf Publishing, Houston.
- Narasimhan, S., Mah, R. S. H., 1987. Generalized likelihood ratio method for gross error identification. *AIChE J.* 33 (9), 1514–1521.
- Narasimhan, S., Shah, S. L., 2008. Model identification and error covariance matrix estimation from noisy data using PCA. *Cont. Eng. Prac.* 16, 146–155.
- Noble, B., Daniel, J. W., 1977. *Applied Linear Algebra.* Englewood Cliffs, N.J., Prentice-Hall Inc.
- Nounou, M. N., Nounou, H. N., 2010. Multiscale Latent Variable Regression. *International Journal of Chemical Engineering*, 935315.
- Oppenheim, A., Willsky, A., Nawab, S., Hamid, W., Young, I., 1997. *Signals & Systems.* Prentice-Hall signal processing series. Prentice Hall.
- Razak, R. A., Bhushan, M., Belur, M. N., Tiwari, A. P., Kelkar, M. G., Pramanik, M., 2012. Data reconciliation and gross error analysis of self powered neutron detectors: comparison of PCA and IPCA based models. *Int. J. Adv. Eng. Sci. Appl. Math.* 4, 91–115.
- Reis, M. S., 2009. A multiscale empirical modeling framework for system identification. *Journal of Process Control* 19 (9), 1546–1557.
- Rhinehart, R. R., 1991. Method for automatic adaptation of the time constant for a first-order filter. *Industrial & Engineering Chemistry Research* 30 (1), 275–277.
- Romagnoli, J., Sanchez, M., 1999. *Data Processing and Reconciliation for Chemical Process Operations.* ISSN. Elsevier Science.
- Sheriff, M. Z., Mansouri, M., Karim, M. N., Nounou, H., Nounou, M., 2017. Fault detection using multiscale pca-based moving window glrt. *Journal of Process Control* 54, 47 – 64.
- Sinha, R. K., Kakodkar, A., 2006. Design and development of the AHWR - the Indian thorium fuelled innovative nuclear reactor. *Nucl. Eng. and Design* 236 (7-8), 683–700.
- T, A. G. S., 1975. Checking and correction of measurements on the basis of linear system model. *PROBL. CONTROL INFORM. THEORY; HUNGARY; DA.* 1975; VOL. 4; NO 1; PP. 57-69; ABS. RUSSE; BIBL. 11 REF.
- Uhrig, R. E., Tsoukalas, L. H., 1999. Soft computing technologies in nuclear engineering applications. *Prog. Nucl. Energy* 34 (1), 13 – 75.
- Upadhyaya, B. R., Mehta, C., Bayram, D., Oct 2014. Integration of time series modeling and wavelet transform for monitoring nuclear plant sensors. *IEEE Trans. Nucl. Sci.* 61 (5), 2628–2635.
- Upadhyaya, B. R., Zhao, K., Lu, B., 2003. Fault monitoring of nuclear power plant sensors and field devices. *Prog. Nucl. Energy* 43, 337–342.
- Vaclavek, V., 1969. Studies on system engineering. II. on the application of the calculus of observations in calculations of chemical engineering balances. *Collect. Czech. Chem. Commun.* 34 (2), 364–372.
- Vajpayee, V., Mukhopadhyay, S., Tiwari, A. P., 2018. Multiscale subspace identification of nuclear reactor using wavelet basis function. *Annals of Nuclear Energy* 111, 280 – 292.
- Venkatasubramanian, V., Rengaswamy, R., Kavuri, S. N., 2003a. A review of process fault detection and diagnosis: Part II: Qualitative models and search strategies. *Comp. & Chem. Eng.* 27 (3), 313–326.
- Venkatasubramanian, V., Rengaswamy, R., Kavuri, S. N., Yin, K., 2003b. A review of process fault detection and diagnosis: Part III: Process history based methods. *Comp. & Chem. Eng.* 27 (3), 327–346.
- Venkatasubramanian, V., Rengaswamy, R., Yin, K., Kavuri, S. N., 2003c. A review of process fault detection and diagnosis: Part I: Quantitative model-based methods. *Comp. & Chem. Eng.* 27 (3), 293–311.
- Weber, R., 1980. Measurement smoothing with a nonlinear exponential filter. *AIChE Journal* 26 (1), 132–134.
- Willisky, A. S., 1976. A survey of design methods for failure detection in dynamic systems. *Automatica* 12 (6), 601–611.
- Yellapu, V. S., Mishra, A. K., Tiwari, A. P., Degweker, S. B., 2015a. Online Fault Detection and Diagnosis of In-Core Neutron Detectors Using Generalized Likelihood Ratio Method. *IEEE Trans. Nucl. Sci.* 62 (6), 3311–3323.
- Yellapu, V. S., Tiwari, A. P., Degweker, S. B., 2015b. Application of data reconciliation and fault detection and isolation of ion chambers in Advanced Heavy Water Reactor. *Ann. Nucl. Energy* 85, 1210–1225.
- Yellapu, V. S., Tiwari, A. P., Degweker, S. B., Sept 2015c. An iterative principal component test for fault detection and isolation. In: 2015 IEEE Conference on Control Applications (CCA). pp. 972–977.
- Yellapu, V. S., Tiwari, A. P., Degweker, S. B., 2017. Application of data reconciliation for fault detection and isolation of in-core self-powered neutron detectors using iterative principal component test. *Prog. Nucl. Energy* 100, 326 – 343.
- Yellapu, V. S., Tiwari, A. P., Shimjith, S. R., Naskar, M., Degweker, S. B., Aug 2013. Space-time kinetics modeling for the determination of neutron detector signals in Advanced Heavy Water Reactor. In: 2013 IEEE Int. Conf. Control App. (CCA). pp. 1224–1229.
- Yellapu, V. S., Vajpayee, V., Tiwari, A. P., July 2019. Online Fault Detection and Isolation in Advanced Heavy Water Reactor Using Multiscale Principal Component Analysis. *IEEE Trans. Nucl. Sci.* 66 (7), 1790–1803.
- Yoon, S., MacGregor, J. F., 2004. Principal-component analysis of multiscale data for process monitoring and fault diagnosis. *AIChE Journal* 50 (11), 2891–2903.
- Zhao, K., Upadhyaya, B. R., 2006. Model based approach for fault detection and isolation of helical coil steam generator systems using principal component analysis. *IEEE Trans. Nucl. Sci.* 53 (4), 2343–2352.